ARTICLES
https://doi.org/10.1038/s41593-020-00762-9
nature neuroscience

Check for updates

Maternal immune activation in mice disrupts proteostasis in the fetal brain

Brian T. Kalish[1,2,9]✉, Eunha Kim[3,9], Benjamin Finander[1,2], Erin E. Duffy[1], Hyunju Kim[3], Casey K. Gilman[3], Yeong Shin Yim[4,5], Lilin Tong[2,6], Randal J. Kaufman[7], Eric C. Griffith[1], Gloria B. Choi[4,5], Michael E. Greenberg[1]✉ and Jun R. Huh[3,8]✉

Maternal infection and inflammation during pregnancy are associated with neurodevelopmental disorders in offspring, but little is understood about the molecular mechanisms underlying this epidemiologic phenomenon. Here, we leveraged single-cell RNA sequencing to profile transcriptional changes in the mouse fetal brain in response to maternal immune activation (MIA) and identified perturbations in cellular pathways associated with mRNA translation, ribosome biogenesis and stress signaling. We found that MIA activates the integrated stress response (ISR) in male, but not female, MIA offspring in an interleukin-17a-dependent manner, which reduced global mRNA translation and altered nascent proteome synthesis. Moreover, blockade of ISR activation prevented the behavioral abnormalities as well as increased cortical neural activity in MIA male offspring. Our data suggest that sex-specific activation of the ISR leads to maternal inflammation-associated neurodevelopmental disorders.

Fetal brain development is exquisitely sensitive to environmental influence. Transcriptional programs in the fetal brain regulate complex and overlapping developmental processes that ultimately shape the functional architecture of the adult brain. Perturbations in the intrauterine environment can therefore have profound and long-lasting effects on neurodevelopment[1–3]. Epidemiological data suggest that significant maternal infections during pregnancy are associated with an increased risk of neurodevelopmental and neuropsychiatric diseases in offspring[4–7]. However, our understanding of the molecular mechanisms underpinning the detrimental effects of adverse environmental exposures on the development of the fetal brain remains limited.

This phenomenon has been studied in a rodent MIA model in which offspring of pregnant mice intraperitoneally injected with a mimetic of viral infection (synthetic double-stranded RNA (dsRNA), polyinosinic:polycytidylic acid (poly(I:C)) exhibit pronounced neurodevelopmental consequences, including impaired social interaction and repetitive behavior[8–10]. MIA-induced disruption of offspring neurodevelopment requires maternal type 17 helper T (T_H17) cell and interleukin-17a (IL-17a) pathways[9]; however, the signaling mechanisms downstream of IL-17a that give rise to MIA-associated neurodevelopmental phenotypes remain unclear.

In this study, we used a combination of single-cell transcriptomics and ribosome profiling to systematically quantify transcriptional and translational changes in MIA offspring. We found that MIA was associated with cell type- and sex-specific transcriptional alterations in the fetal brain, and we identified a widespread disruption in the expression of genes involved in mRNA translation. These effects were associated with activation of the ISR via phosphorylation of the α-subunit of eukaryotic translation initiation factor 2 (eIF2α), which led to sex-specific arrest of mRNA translation in the fetal brain. ISR dysregulation has previously been implicated in neurodegenerative conditions, including frontotemporal dementia and amyotrophic lateral sclerosis, as well as the behavioral and neurophysiological abnormalities associated with Down syndrome[11–14]. Strikingly, genetic reduction of phospho-eIF2α levels and pharmacological blockade of ISR activation in the developing fetus protected against MIA-associated behavioral abnormalities. Together, our findings provide new insight into the implications of aberrant intrauterine ISR activation for MIA-associated neurodevelopmental conditions and broaden our understanding of the mechanisms by which intrauterine stress shapes neurodevelopment.

Results

Single-cell RNA sequencing of the fetal brain exposed to maternal inflammation. The development of the fetal cortex requires precise temporal and spatial coordination of gene expression and mRNA translation. To gain insight into the cell-type-specific effects of MIA on the developing fetal brain, we employed high-throughput single-cell RNA sequencing (scRNA-seq) to profile gene expression in the fetal cortex of both male and female fetuses at embryonic days 14.5 and 18.5 (E14.5 and E18.5) in the context of MIA or a sham saline control treatment (PBS) (Fig. 1a). These time points were selected to survey critical periods in fetal brain maturation following poly(I:C) administration at E12.5. After quality and doublet filtering (quality metrics provided in Extended Data Fig. 1a), we analyzed the transcriptomes of 37,377 cells at E14.5 and 57,953

[1]Department of Neurobiology, Blavatnik Institute, Harvard Medical School, Boston, MA, USA. [2]Division of Newborn Medicine, Department of Pediatrics, Boston Children's Hospital, Boston, MA, USA. [3]Department of Immunology, Blavatnik Institute, Harvard Medical School, Boston, MA, USA. [4]The Picower Institute for Learning and Memory, Massachusetts Institute of Technology, Cambridge, MA, USA. [5]Department of Brain and Cognitive Sciences, Massachusetts Institute of Technology, Cambridge, MA, USA. [6]Department of Molecular Genetics, University of Toronto, Toronto, Ontario, Canada. [7]Degenerative Disease Program, Sanford Burnham Prebys Medical Discovery Institute, La Jolla, CA, USA. [8]Evergrande Center for Immunologic Diseases, Harvard Medical School and Brigham and Women's Hospital, Boston, MA, USA. [9]These authors contributed equally: Brian T. Kalish, Eunha Kim.
✉e-mail: brian.kalish@childrens.harvard.edu; michael_greenberg@hms.harvard.edu; Jun_Huh@hms.harvard.edu

cells at E18.5, recovering an average of 3,529 and 2,168 unique transcripts per cell, respectively.

Standard graph-based clustering methods were used to classify E14.5 and E18.5 samples into 22 and 24 transcriptionally distinct cell types, respectively, which were assigned identities based on canonical marker gene expression (Fig. 1b,c). This analysis resolved developmental, anatomical and functional cell states in the cortex, including proliferative neural precursors, migratory radial glia, as well as intermediate and mature neuronal subtypes. Moreover, further clustering of major cell classes served to reveal additional developmental and functional cellular subtype heterogeneity. At E14.5, we identified major cortical layer subtypes, interneurons, cortical plate, cortical subplate, migrating and proliferating subventricular zone (SVZ) cells, as well as multiple radial glia subtypes, all with distinct transcriptional signatures (Extended Data Fig. 1b–h). At E18.5, we identified increased diversity of cortical layer, interneuronal and striatal subtypes compared with at E14.5 (Extended Data Fig. 2a–e). Together, the developmental hierarchy of our cell type classifications were in broad agreement with previous scRNA-seq data from the embryonic mouse brain[15].

We analyzed male and female offspring independently given previously described sex differences in the MIA phenotype[16,17]. While MIA did not dramatically alter the distribution of cell types in male or female mice, differential gene expression (DGE) analysis between MIA and PBS subpopulations within defined cell types revealed profound, widespread gene expression changes in MIA samples (Supplementary Tables 1–9). We used a false discovery rate (FDR) value of <0.05 to define statistically significant changes in gene expression between MIA and control offspring. We were able to identify both shared and cell-type-specific MIA-associated gene signatures at both E14.5 and E18.5 in neuronal and non-neuronal subtypes (Fig. 1d,e and Extended Data Fig. 3). For example, the expression levels of genes regulating translation were commonly decreased in the cortical excitatory and inhibitory neurons of MIA male offspring compared with those of PBS male or MIA female offspring (Fig. 1e). Gene Ontology (GO) analysis of differentially expressed genes in select cell types suggested widespread disruption of networks associated with mRNA trafficking and cytoplasmic translation (Fig. 1f). We identified altered transcription of numerous eukaryotic translation initiation and elongation factors across several cell types when comparing MIA males and PBS males. Specifically, when comparing MIA males with PBS males in layer II–IV cortical neurons at E18.5, we found decreased expression of *Eif3e*, *Eif3k*, *Eef2* and *Eef1g*, all of which are critical for protein synthesis (Fig. 1g). In this same cell cluster, we identified decreased expression of several transfer RNA synthetases in MIA males, including *Farsb* and *Nars* (Fig. 1g). Aminoacyl-tRNA synthetase factors help maintain translational fidelity and are essential components of the protein biosynthesis machinery[18]. Finally, we identified decreased expression of *Eif2s1* in MIA males, which encodes eIF2α, which is a central regulatory protein in cellular translation (Fig. 1g). Additionally, many genes encoding ribosomal subunits (for example, *Rps8*, *Rps10* and *Rpl13*) were downregulated in MIA male offspring relative to PBS male offspring at E14.5, and to a lesser extent at E18.5 (Fig. 2a and Extended Data Fig. 4a).

Interestingly, we found that a large proportion of the transcriptional effects of MIA on male mice were sex-dependent; that is, male and female MIA offspring demonstrated prominent differences in cell-type-specific gene expression across numerous cell types (Fig. 1e,h and Extended Data Fig. 3). We applied a multifactor statistical analysis to identify genes with altered cell-type-specific expression changes with MIA exposure between males and females. Similar to comparisons between MIA and PBS male offspring, MIA male offspring exhibited profound changes in ribosomal-, stress- and translation-associated genes across many cell types compared to MIA female offspring (Fig. 2b and Extended Data Fig. 4b). At E14.5 in particular, male MIA offspring demonstrated a near-global reduction in expression of ribosomal-subunit genes compared with male PBS offspring, whereas female MIA offspring demonstrated few changes in ribosomal subunit genes compared with female PBS offspring (Extended Data Fig. 4c,d). Comparisons between PBS male and female offspring revealed some sex-specific expression of ribosomal-subunit genes in select cell types at E14.5 and E18.5, but these changes were far less prevalent than in the MIA male with PBS male or MIA female comparisons (Extended Data Fig. 5). A GO analysis of differentially expressed genes in the multifactor analysis between MIA males and females revealed several broad and cell-type-specific functional pathways, but the regulation of translation emerged as a common biologic process altered in many cell types (Fig. 1i). For example, in layer II–IV cortical neurons, we found sex-dependent expression of *Ttf1*, which is a nucleolar protein involved in the Pol-I-mediated transcription of ribosomal genes and ribosome biogenesis[19,20] (Fig. 1j). When compared within sex groups, *Ttf1* was increased in MIA males (FDR = 3.1×10^{-5}) and decreased in MIA females (FDR = 1.5×10^{-51}) relative to sex-matched PBS controls. We also found sex-dependent expression of the stress-responsive factors ATF4 (decreased in MIA females relative to PBS females, FDR = 0.033) and ATF7 (decreased in MIA females relative to PBS females, FDR = 1.04×10^{-19}) (Fig. 1j). ATF4 controls the expression of adaptive genes that facilitate cell survival

Fig. 1 | Single-cell sequencing of the fetal brain at E14.5 and E18.5 in the setting of MIA. a, Schematic overview of the experimental design, including dissociation of embryonic cortices, single-cell encapsulation and library preparation. **b**, UMAP of all analyzed E14.5 cells, with cell types labeled by color ($n = 22$ clusters). Data from $n = 2$ mice per group. **c**, UMAP of all analyzed E18.5 cells, with cell types labeled by color ($n = 24$ clusters). Data from $n = 2$ mice per group. **d**, Strip plot displaying DGE between MIA male offspring and PBS male offspring at E14.5. Colored dots represent significant genes (FDR < 0.05). The *x* axis displays select cortical cell types. Data from $n = 2$ mice per group. **e**, Heatmap of single-cell gene expression changes of select genes in two cell types at E14.5: *Neurod2*-positive cortical excitatory neurons (A) and *Gad2*-positive inhibitory neurons (B). Comparisons labeled 'PBS male' are pairwise comparisons between PBS males and MIA males. For these comparisons, blue corresponds to increased expression in MIA males, while pink corresponds to decreased expression in MIA males. Comparisons labeled 'MIA female' are multifactor comparisons measuring the difference between the changes in expression with MIA between male and female mice. For these comparisons, blue corresponds to an increase in the difference between MIA and PBS expression levels in males, while pink corresponds to a decrease in this difference. Data from $n = 2$ mice per group. **f**, GO analysis of differentially expressed genes (FDR < 0.05) between MIA and PBS male offspring in select cell types at E14.5. The *x* axis displays the fold-enrichment relative to the reference gene set. Data from $n = 2$ mice per group. **g**, Volcano plot of MIA-dependent gene expression in layer II–IV cluster A neurons at E18.5. Colored dots indicate statistical significance (FDR < 0.05). Positive $\log_2$(FC) (red dots) indicates higher gene expression in PBS males (M) relative to MIA males, and negative $\log_2$(FC) (blue dots) indicates higher gene expression in MIA males relative to PBS males. Data from $n = 2$ mice per group. **h**, Strip plot displaying sex-dependent gene expression in MIA offspring at E14.5. Colored dots represent significant genes (FDR < 0.05). The *x* axis displays select cortical cell types. Data from $n = 2$ mice per group. **i**, GO analysis of sex-dependent genes in MIA offspring in select cell types at E14.5 (FDR < 0.05). The *x* axis displays the fold-enrichment relative to the reference gene set. Data from $n = 2$ mice per group. **j**, Volcano plot of sex-dependent gene expression in MIA male and female (F) offspring in layer II–IV cluster A neurons at E18.5. Colored dots indicate statistical significance (FDR < 0.05) by interaction term analysis to identify genes that vary by sex with MIA exposure. Negative $\log_2$(FC) values indicate Δ(PBS M – MIA M) < Δ(PBS F – MIA F). Data from $n = 2$ mice per group.

during periods of stress, such as hypoxia or starvation, and has been implicated in neurodegeneration[21]. These findings suggest that MIA may induce cell-type- and sex-specific transcriptional alterations in the fetal brain.

MIA disrupts protein synthesis in the fetal brain. Given our finding that cytoplasmic translation was a common pathway dysregulated in male MIA offspring, we sought to directly assess the effects of MIA on global protein synthesis in the fetal mouse brain. We employed a modified version of the previously described surface sensing of translation (SUnSET) method[22]. In this approach, the puromycin analog *O*-propargyl-puromycin (OPP) serves as a structural mimic of aminoacyl-tRNAs and is incorporated into nascent polypeptide chains[22]. OPP labeling per-

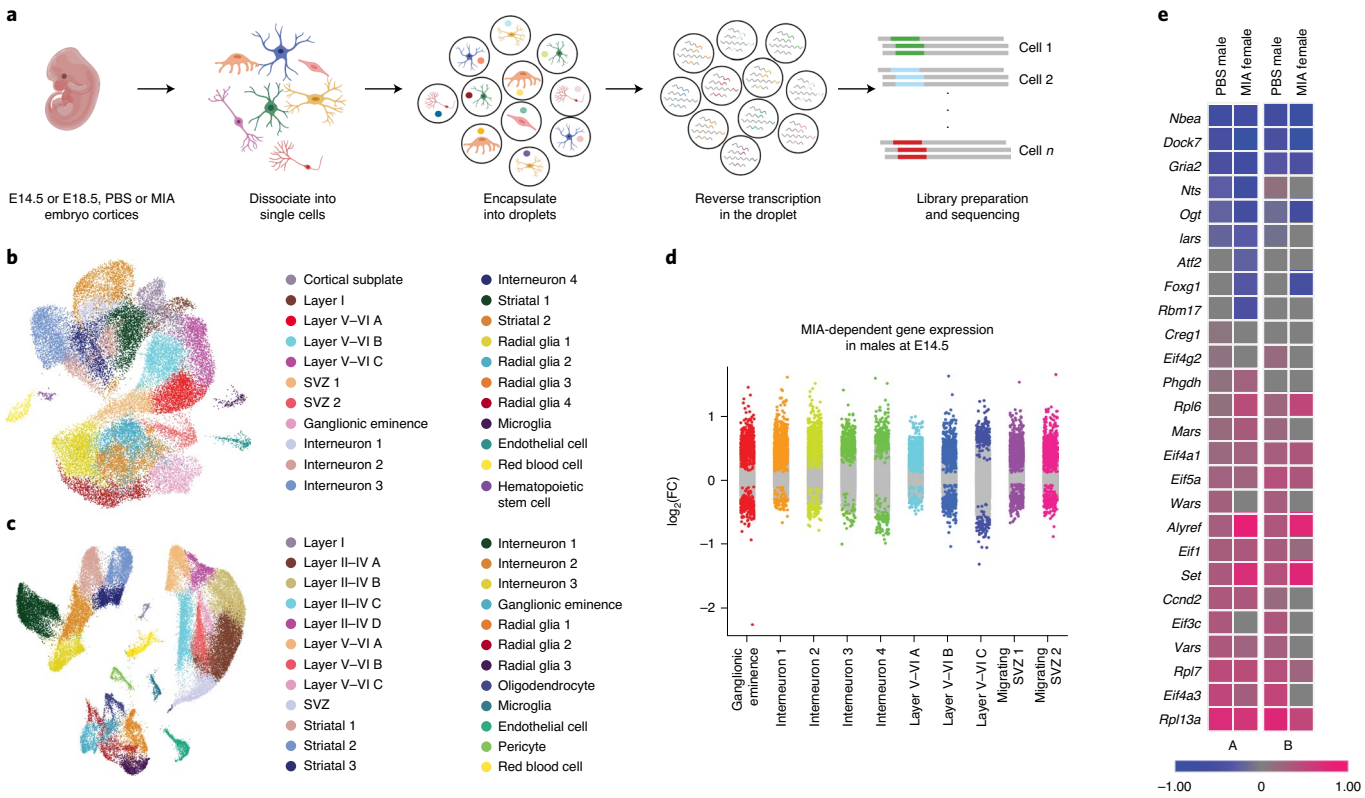

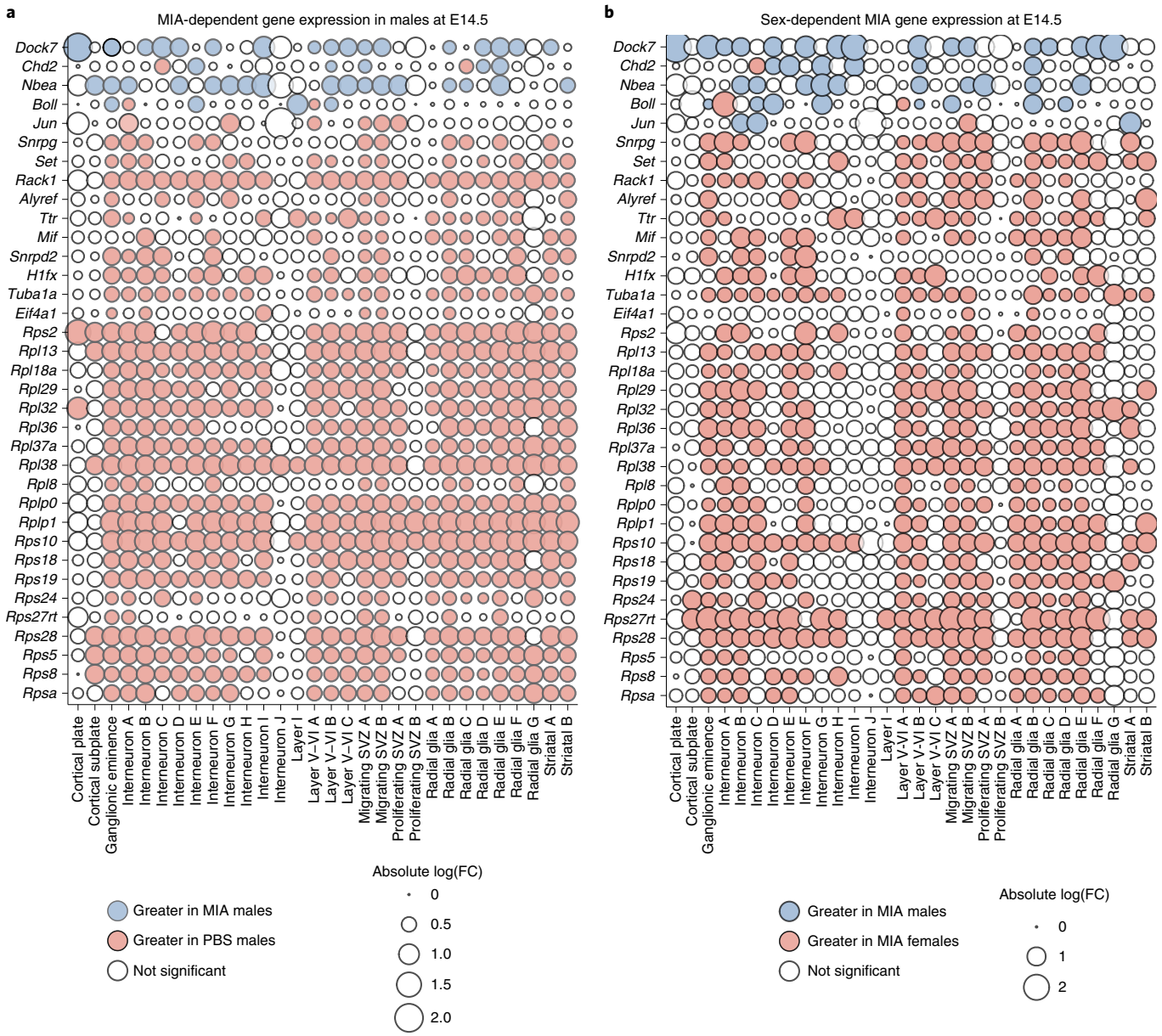

Fig. 2 | Single-cell DGE changes at E14.5. a, Bubble plot of highly variable genes between MIA and PBS male offspring at E14.5, demonstrating a widespread decrease in the expression of multiple ribosomal subunits in MIA male offspring. All significant genes had FDR values of <0.05. Blue indicates an increase in MIA males while red indicates an increase in PBS males. Data from $n = 2$ mice per group. **b**, Bubble plot of sex-dependent genes in MIA offspring at E14.5, demonstrating a widespread decrease in the expression of multiple ribosomal subunits in MIA male offspring. All significant genes had FDR values of <0.05. Blue indicates an increase in Δ(MIA males – PBS males) while red indicates an increase in Δ(MIA females – PBS females). Data from $n = 2$ mice per group.

mits subsequent fluorescent tagging of the modified polypeptides via a click-chemistry reaction, thereby enabling the quantitative measurement of protein synthesis within tissues. Fetal cortical tissue from E18.5 controls and MIA offspring were incubated with OPP, followed by a click-chemistry reaction with tetramethylrhodamine (TAMRA) azide and subsequent SDS–polyacrylamide gel electrophoresis (PAGE). Protein synthesis was quantified by comparing the TAMRA signal (new protein) over the Coomassie signal (total protein). We found that nascent protein synthesis was decreased only in the cortex of male MIA offspring (Fig. 3a). This finding was consistent with our scRNA-seq data, which suggested that there are deficits in ribosome-subunit expression in MIA male offspring.

Activation of the ISR in male MIA offspring. To explain the finding that there is a significant reduction in nascent protein synthesis in MIA male fetal brains, we hypothesized that alterations in fetal brain translation in response to MIA might be due to activation of the ISR. The ISR is an adaptive mechanism that can be activated under physiologic or pathologic conditions to execute a global reduction in protein synthesis as a means to shift resources toward cell survival. The phosphorylation of eIF2α at serine 51 is the critical regulatory hub in the activation of the ISR[23] (Fig. 3b). Probing with an eIF2α phospho-specific antibody, we found a strong induction of eIF2α phosphorylation specifically in the brain of male MIA offspring (Fig. 3c). By contrast, we observed no changes in the levels of ribosomal protein S6 kinase

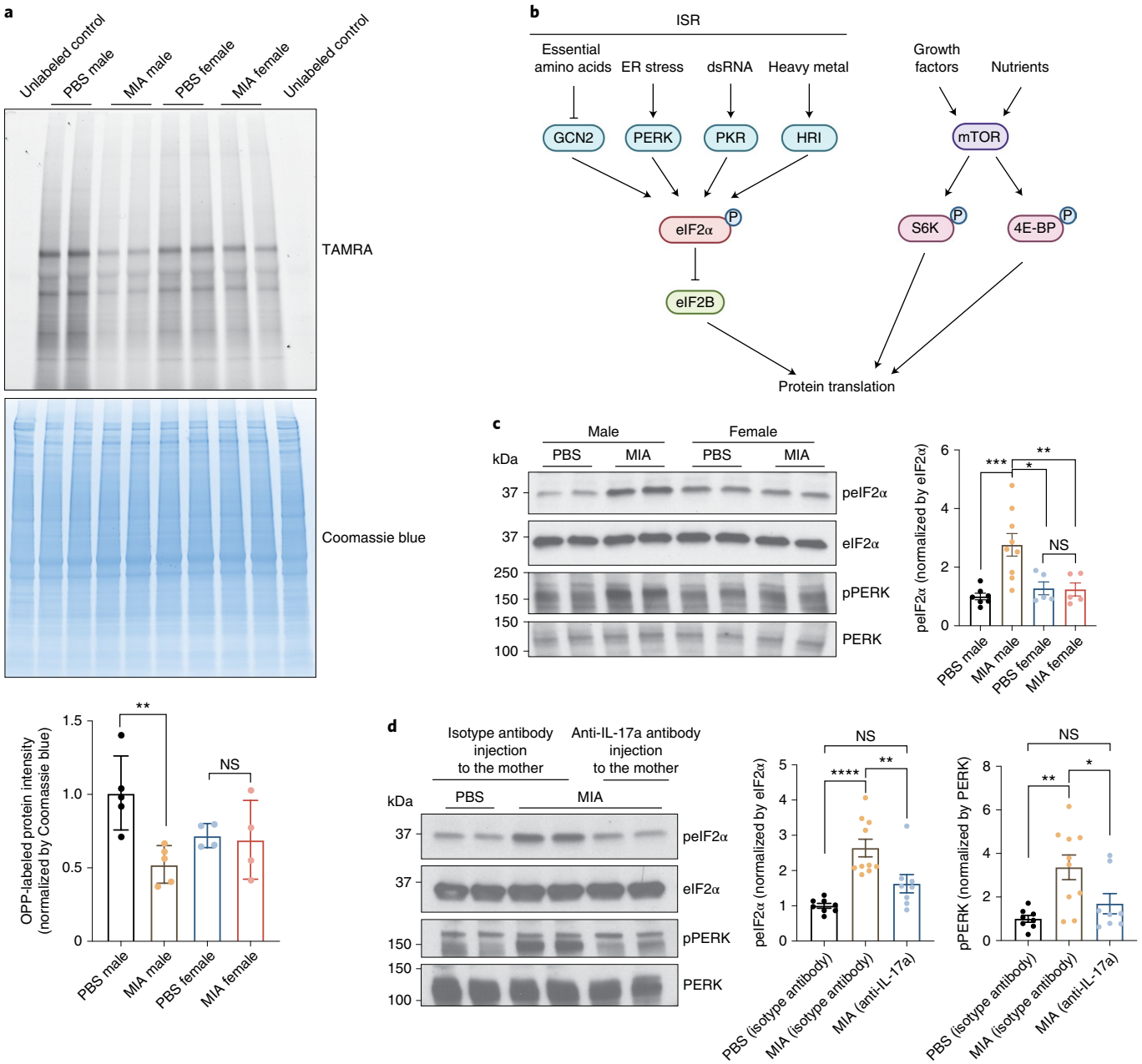

Fig. 3 | MIA inhibits protein translation in the fetal brain via the ISR. a, Images (top) and quantification (bottom) of TAMRA-conjugated proteins labeled by OPP, extracted and isolated by SDS–PAGE and analyzed by fluorescence scanning at 532 nm. A representative section of Coomassie-stained gel is shown for loading comparison (two-way ANOVA: sex (male or female) × stimulus (PBS or MIA) interaction, $F_{1,14} = 5.874$, $P = 0.0295$; effect of sex, $F_{1,14} = 0.4167$, $P = 0.5290$; effect of stimulus, $F_{1,14} = 7.462$, $P = 0.0162$, followed by Tukey's multiple comparisons test: PBS male versus MIA male, $^{**}P = 0.0082$; $n = 5$ PBS male and 5 MIA male mice, $n = 4$ PBS female and 4 MIA female pups; 3 independent litters for PBS, 2 independent litters for MIA). NS, not significant. **b**, Schematic representation of the regulation of translation initiation through eIF2α-dependent regulation and mTOR-dependent regulation. **c**, Immunoblot image (left) analysis measuring phospho-eIF2α (peIF2α) and phospho-PERK (pPERK) levels and quantification (right) for phospho-eIF2α in E18.5 PBS and MIA fetal cortices. The *y* axis represents the relative blot intensity to PBS male control mice (two-way ANOVA: sex (male or female) × stimulus (PBS or MIA) interaction, $F_{1,22} = 8.229$, $P = 0.0089$; effect of sex, $F_{1,22} = 3.939$, $P = 0.0598$; effect of stimulus, $F_{1,22} = 7.567$, $P = 0.0117$, followed by Tukey's multiple comparisons test: PBS male versus MIA male, $^{***}P = 0.0009$, PBS female versus MIA male, $^{*}P = 0.0118$, MIA male versus MIA female, $^{**}P = 0.0097$; $n = 7$ PBS male mice, $n = 9$ MIA male mice, $n = 5$ PBS female and 5 MIA female pups; 3 independent litters). **d**, Immunoblot image (left) analysis measuring phospho-eIF2α and phospho-PERK levels and quantification (right) for phospho-eIF2α in isotype-antibody treated or IL-17a-blocking-antibody-treated E18.5 PBS and MIA fetal cortices. The *y* axis represents the relative blot intensity to the isotype-antibody-treated PBS control (phospho-eIF2α: one-way ANOVA, $F_{2,23} = 14.88$, $P = 7.14 \times 10^{-5}$, Tukey's multiple comparisons test: PBS isotype antibody versus MIA isotype antibody, $^{****}P = 5.58 \times 10^{-5}$, MIA isotype antibody versus MIA anti-IL-17a, $^{**}P = 0.0083$; phospho-PERK: one-way ANOVA, $F_{2,23} = 7.259$, $P = 0.0036$, Tukey's multiple comparisons test: PBS isotype antibody versus MIA isotype antibody, $^{**}P = 0.0036$; MIA isotype antibody versus MIA anti-IL-17a, $^{*}P = 0.0423$; $n = 8$ mice each for PBS isotype antibody and MIA anti-IL-17a, $n = 10$ mice for MIA isotype antibody; 3 independent litters). Data are shown as the mean ± s.e.m.; see Supplementary Table 20 for detailed statistics. Unprocessed blots are provided in the source data.

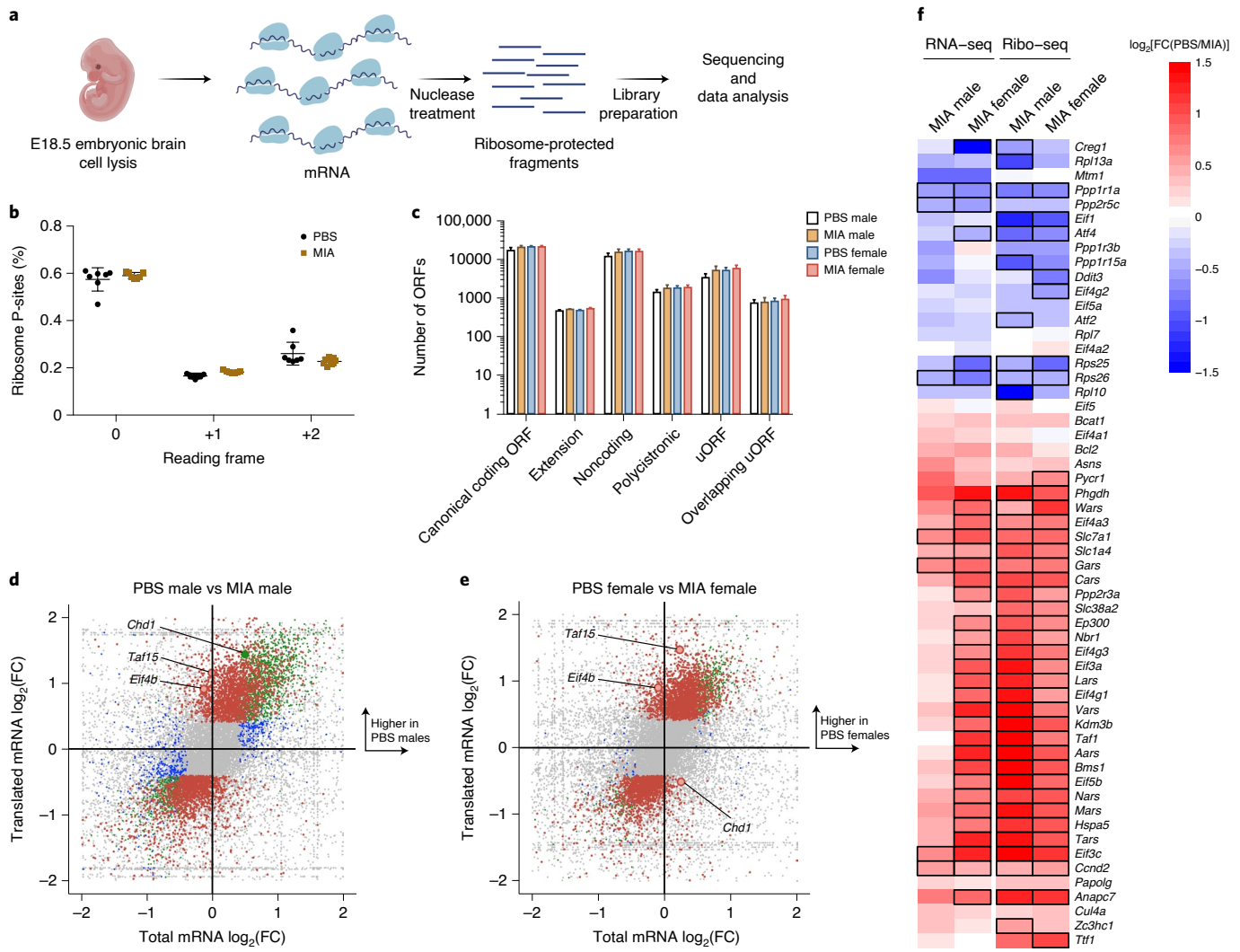

Fig. 4 | Alterations in the translational landscape of the MIA fetal brain. a, Schematic of experimental approach for ribosome profiling. **b**, The percentage of ribosome-profiling reads in frame 0 by experimental condition. Data are shown as the mean ± s.e.m. Data are from $n = 7$ PBS and $n = 7$ MIA mice, each from 2 independent litters. **c**, Bar graph of ORF subtypes based on transcript types and ORF locations between all experimental groups. Data are shown as the mean ± s.e.m. For individual data underlying this plot, see Supplementary Table 21. Data are from $n = 7$ PBS and $n = 7$ MIA mice, each from 2 independent litters. **d**, Quadrant plot of transcriptional and translational changes in MIA male offspring compared with PBS male offspring. Genes significant only in the total mRNA-seq are in blue, genes significant only in the ribo-seq are in red, and genes significant in both are in green. Significant transcripts have a FDR value of <0.05. Positive $\log_2$(FC) values indicate an increase in the PBS group. Data are from $n = 7$ PBS and $n = 7$ MIA mice, each from 2 independent litters. **e**, Quadrant plot of transcriptional and translational changes in MIA female offspring compared with PBS female offspring. Transcripts significant only in the total mRNA-seq are in blue, transcripts significant only in the ribo-seq are in red, and transcripts significant in both are in green. Significant transcripts have a FDR value of <0.05. Positive $\log_2$(FC) values indicate an increase in the PBS group. Data are from $n = 7$ PBS and $n = 7$ MIA mice, each from 2 independent litters. **f**, Heatmap of $\log_2$(FC) values of transcriptional (RNA-seq) and translational (ribo-seq) changes in MIA males and females relative to sex-matched PBS controls. Genes are known targets of the ISR response to chronic stress[49] and the translational machinery. Black outlines indicate statistically significant (FDR < 0.05) changes relative to corresponding sex-matched PBS controls in a multifactor edgeR analysis. Positive $\log_2$(FC) values, shown in red, indicate an increase in the PBS group, while negative $\log_2$(FC) values, shown in blue, indicate an increase in the MIA group. Data are from $n = 7$ PBS and $n = 7$ MIA mice, each from 2 independent litters.

(S6K) phosphorylation, which is a distinct point of translational control (Extended Data Fig. 6a).

eIF2α phosphorylation can be triggered by a diverse array of cellular stressors[23] and is mediated by four cellular kinases, three of which—protein kinase R (PKR), PKR-like endoplasmic reticulum kinase (PERK) and general control nonderepressible 2 (GCN2)—are present in the brain[24]. The activity of these eIF2α kinases can be monitored via a series of phospho-specific antibody reagents that recognize kinase autophosphorylation that occurs when the kinase is activated. Blotting fetal cortical lysates with these antibodies revealed that PERK, but not PKR or GCN2, was specifically activated in the cortex of male MIA offspring (Fig. 3c and Extended Data Fig. 6b). PERK is triggered by endoplasmic reticulum (ER) stress and the unfolded protein response (UPR), which suggests that these processes are critical signaling mechanisms in MIA[25]. To test whether MIA activates other sensors of the UPR, we performed immunoblotting for inositol-requiring enzyme 1α (IRE1α) and activating transcription factor 6 (ATF6) levels in the E18.5 brain. We found that phosphorylation of IRE1α was increased in the brain of male MIA offspring, while cleaved ATF6 was unchanged (Extended Data Fig. 6c).

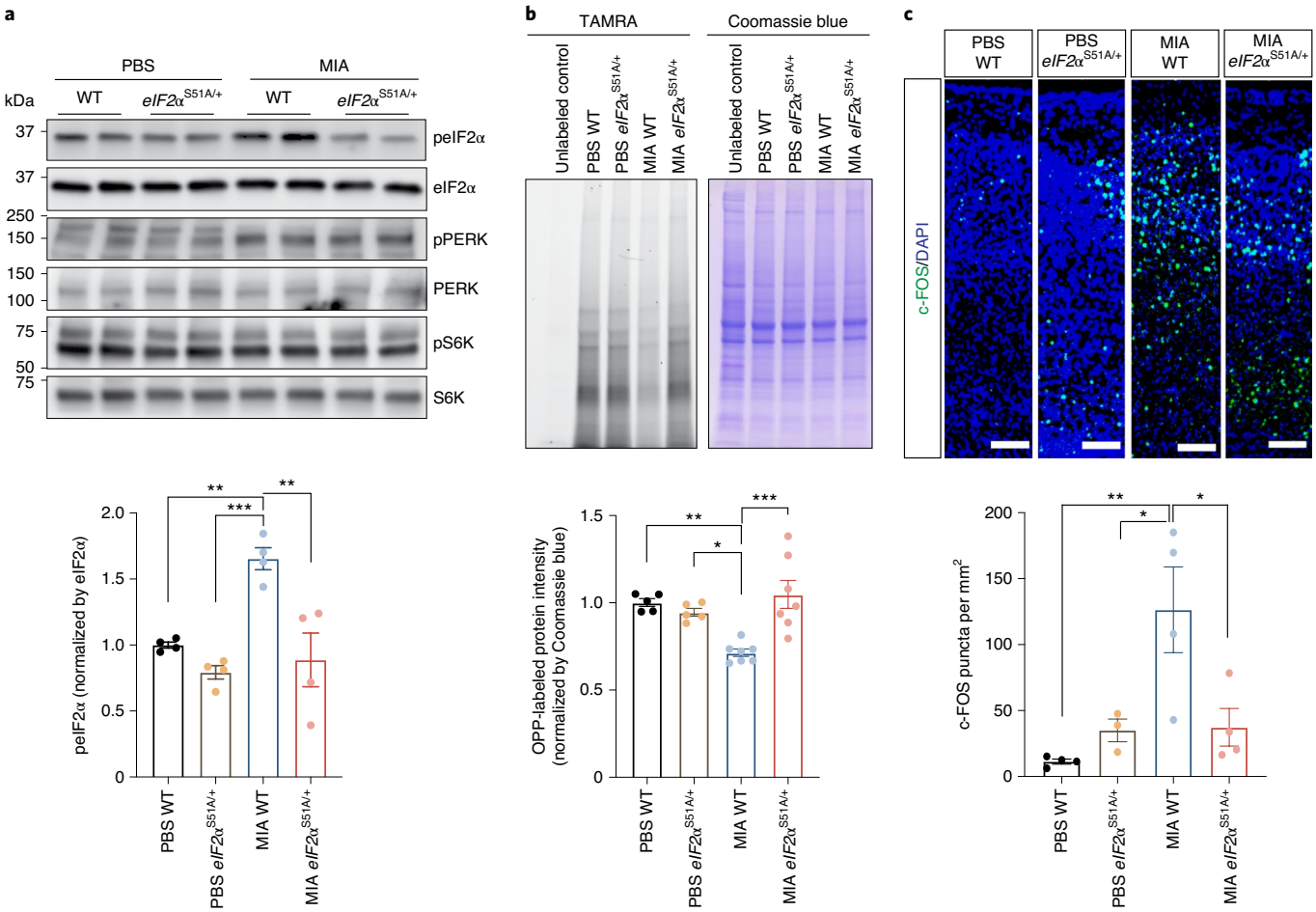

Fig. 5 | Genetic ablation of ISR protects against excessive neural activity in MIA offspring. a, Immunoblot image (top) analysis measuring phospho-eIF2α, phospho-PERK and phospho-S6K (pS6K) levels and quantification (bottom) for phospho-eIF2α in WT and *eIF2α*$^{S51A/+}$ E18.5 male fetal cortices. The *y* axis represents the relative blot intensity to the WT PBS fetal cortices (two-way ANOVA: stimulus (PBS or MIA) × genotype (WT or *eIF2α*$^{S51A/+}$) interaction, $F_{1,12}=6.055$, $P=0.03$; effect of stimulus, $F_{1,12}=10.88$, $P=0.0064$; effect of genotype, $F_{1,12}=18.34$, $P=0.0011$; followed by Tukey's multiple comparisons test: PBS WT versus MIA WT, $^{**}P=0.0073$, MIA WT versus PBS *eIF2α*$^{S51A/+}$, $^{***}P=0.0008$; MIA WT versus MIA *eIF2α*$^{S51A/+}$, $^{**}P=0.0022$; $n=4$ pups from 2 independent litters). **b**, Image (top) and quantification (bottom) of TAMRA-conjugated proteins labeled by OPP, extracted and isolated by SDS-PAGE and analyzed by fluorescence scanning at 532 nm. A representative section of a Coomassie-stained gel is shown for loading comparison (two-way ANOVA: stimulus (PBS or MIA) × genotype (WT or *eIF2α*$^{S51A/+}$) interaction, $F_{1,20}=14.35$, $P=0.0012$; effect of stimulus, $F_{1,20}=3.265$, $P=0.0858$; effect of genotype, $F_{1,20}=7.283$, $P=0.0138$; followed by Tukey's multiple comparisons test: PBS WT versus MIA WT, $^{**}P=0.004$, MIA WT versus PBS *eIF2α*$^{S51A/+}$, $^{*}P=0.0221$; MIA WT versus MIA *eIF2α*$^{S51A/+}$, $^{***}P=0.0004$; $n=5$ PBS WT pups and PBS *eIF2α*$^{S51A/+}$ pups from 3 independent litters, $n=7$ MIA WT pups and MIA *eIF2α*$^{S51A/+}$ pups from 3 independent litters). **c**, Top: representative images of brain tissue from 8–10-week-old mice immunostained for c-Fos. Conditions are MIA and PBS WT and *eIF2α*$^{S51A/+}$ male mice. Scale bar, 100 µm. Bottom: quantification of c-Fos puncta per mm^2 (two-way ANOVA: stimulus (PBS or MIA) × genotype (WT or *eIF2α*$^{S51A/+}$) interaction, $F_{1,11}=8.320$, $P=0.0149$; effect of stimulus, $F_{1,11}=9.007$, $P=0.0121$; effect of genotype, $F_{1,11}=2.798$, $P=0.1226$; followed by Tukey's multiple comparisons test: PBS WT versus MIA WT, $^{**}P=0.0056$; MIA WT versus PBS *eIF2α*$^{S51A/+}$, $^{*}P=0.0373$, MIA WT versus MIA *eIF2α*$^{S51A/+}$, $^{*}P=0.0281$; $n=3$ PBS *eIF2α*$^{S51A/+}$ pups, $n=4$ pups per group for PBS WT, MIA WT and MIA *eIF2α*$^{S51A/+}$; 2 independent litters per group.) Data are shown as the mean ± s.e.m.; see Supplementary Table 20 for detailed statistics. Unprocessed blots are provided in the source data.

We have previously shown that behavioral abnormalities in MIA offspring are mediated by maternal induction of the inflammatory cytokine IL-17a[9]. To test whether activation of ISR in the MIA offspring is dependent on maternal IL-17a, we pretreated pregnant dams with either a control or a IL-17a-blocking antibody 5 h before introducing poly(I:C). Administration of the IL-17a-blocking antibody, but not an isotype-matched control antibody, completely suppressed MIA-induced eIF2α and PERK phosphorylation in the male fetal cortex (Fig. 3d), which demonstrates that PERK-mediated ISR activation in the fetal brain is dependent on maternal IL-17a. Furthermore, previous reports demonstrated that T_H17-cell-inducing mouse commensal bacteria, segmented filamentous bacteria (SFB), is required for maternal induction of the pro-inflammatory cytokine IL-17a after MIA[26,27]. In line with this finding, we did not observe activation of the ISR in the brains of MIA offspring from SFB-negative dams (Extended Data Fig. 7). This result suggests a mechanistic link between the microbiome, maternal IL-17a and the fetal brain stress response.

MIA alters the translational landscape of the fetal brain. Activation of the ISR restructures global mRNA translation in two stages[28]. First, cellular stress induces phosphorylation of eIF2α, which transiently attenuates protein synthesis through inhibition of cap-dependent translation. After resolution of cellular stress, increased expression of GADD34—a regulatory subunit of the phosphatase that dephosphorylates eIF2α—facilitates cap-independent

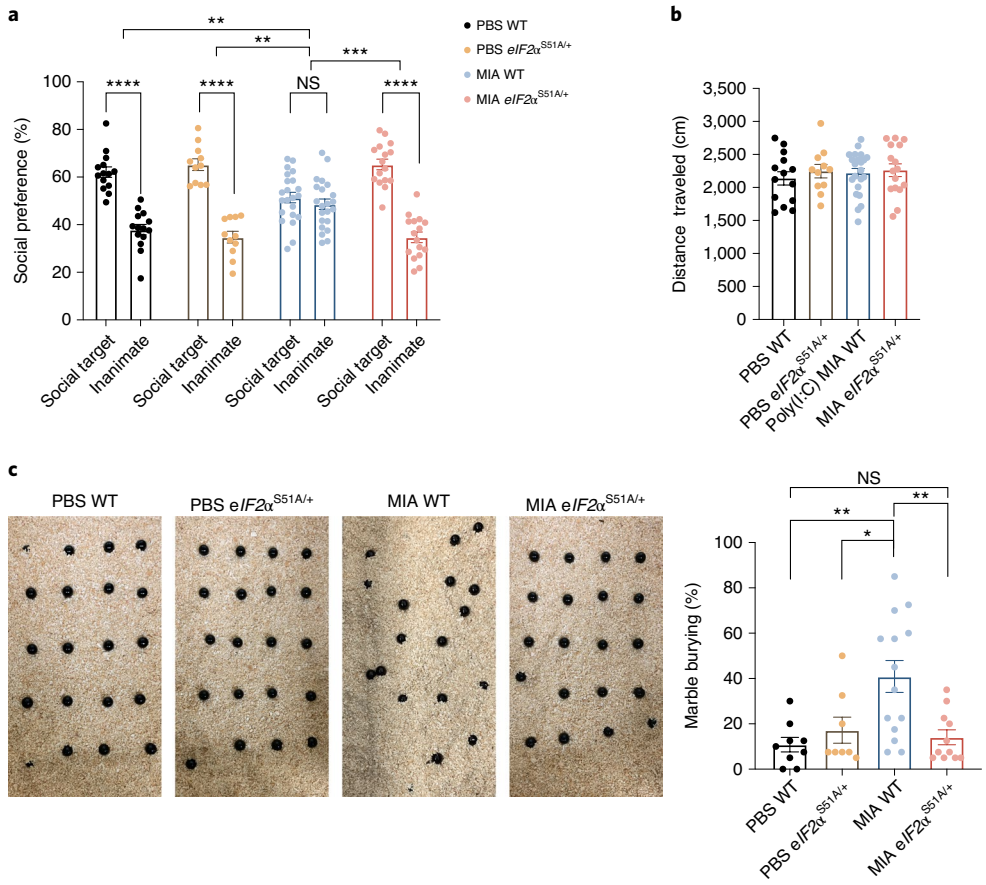

Fig. 6 | Genetic ablation of ISR protects MIA offspring against neurobehavioral abnormalities. a,**b**, Percentage of interaction (**a**) (two-way ANOVA: group (PBS WT, MIA WT, PBS *eIF2*α$^{S51A/+}$ or MIA *eIF2*α$^{S51A/+}$) × preference to the target (social target or inanimate) interaction, $F_{3,118}=19.23$, $P=3.214\times10^{-10}$; effect of preference to the target, $F_{1,118}=170.1$, $P=1.0\times10^{-15}$; followed by Sidak's multiple comparisons test-within group: PBS WT, ****$P=7.9\times10^{-10}$; PBS *eIF2*α$^{S51A/+}$, ****$P=1.19\times10^{-11}$; MIA WT, $P=0.7772$; MIA *eIF2*α$^{S51A/+}$, ****$P=2\times10^{-15}$; two-way ANOVA: stimulus (PBS or MIA) × genotype (WT or *eIF2*α$^{S51A/+}$) interaction, $F_{1,59}=5.275$, $P=0.0252$; effect of stimulus, $F_{1,59}=5.100$, $P=0.0276$; effect of genotype, $F_{1,59}=12.56$, $P=0.0008$; followed by Tukey's multiple comparisons test: PBS WT versus MIA WT, **$P=0.0054$; MIA WT versus PBS *eIF2*α$^{S51A/+}$, ***$P=0.0008$; MIA WT versus MIA *eIF2*α$^{S51A/+}$, ***$P=0.0001$) and total distance moved (**b**) (two-way ANOVA: stimulus (PBS or MIA) × genotype (WT or *eIF2*α$^{S51A/+}$) interaction, $F_{1,59}=0.1195$, $P=0.7308$; effect of stimulus, $F_{1,59}=0.2629$, $P=0.6101$; effect of genotype, $F_{1,59}=0.6928$, $P=0.4086$) in the three-chamber sociability test of WT and *eIF2*α$^{S51A/+}$ adult PBS and MIA offspring littermates ($n=14$ PBS WT mice, $n=11$ PBS *eIF2*α$^{S51A/+}$ mice, $n=22$ MIA WT mice, $n=16$ MIA *eIF2*α$^{S51A/+}$ mice; 4 independent experiments). **c**, Images (left) and quantification (right) of the marble-burying index of WT and *eIF2*α$^{S51A/+}$ adult PBS and MIA offspring littermates (two-way ANOVA: stimulus (PBS or MIA) × genotype (WT or *eIF2*α$^{S51A/+}$) interaction, $F_{1,38}=8.180$, $P=0.0068$; effect of stimulus, $F_{1,38}=5.410$, $P=0.0255$; effect of genotype, $F_{1,38}=3.111$, $P=0.0858$; followed by Tukey's multiple comparisons test: PBS WT versus MIA WT, **$P=0.0025$; MIA WT versus PBS *eIF2*α$^{S51A/+}$, *$P=0.0292$; MIA WT versus MIA *eIF2*α$^{S51A/+}$, **$P=0.0045$; $n=9$ PBS WT mice, $n=8$ PBS *eIF2*α$^{S51A/+}$ mice, $n=14$ MIA WT mice, $n=11$ MIA *eIF2*α$^{S51A/+}$ mice; 3 independent experiments). Data are shown as the mean ± s.e.m.; see Supplementary Table 20 for detailed statistics.

translation of stress-adaptive transcripts, while also feeding back to promote dephosphorylation of eIF2α[29]. Stress-adaptive transcripts necessary to promote cell survival are translated through cap-independent mechanisms, including internal ribosome entry site (IRES) and alternative initiation mechanisms[28].

We sought to measure the changes associated with MIA in this dynamic process at codon-level resolution. Therefore, we performed deep sequencing of ribosome-protected mRNA fragments (ribo-seq) at E18.5 in parallel with bulk RNA-seq from the same biologic sample[30] (Fig. 4a and Supplementary Tables 9–19). DNA libraries prepared from ribosome-protected mRNA fragments using established methods[30] were sequenced to a depth of ~80 million reads per sample and showed expected periodicity indicative of high-quality ribosome profiling (Fig. 4b). We characterized the translated open reading frames (ORFs) based on transcript types and ORF locations, including canonical ORFs, upstream ORFs in 5′ untranslated regions (uORFs), downstream ORFs in 3′ untranslated regions (dORFs) and annotated noncoding ORFs (ncORFs) using RiboORF[31] (Fig. 4c). Although some studies have suggested that acute ISR increases the usage of uORFs, we did not observe any statistically significant differences in the distribution of expression between experimental groups for any of the ORF classes. Such changes in uORF utilization may occur earlier than the selected E18.5 time point. We identified transcripts with significant changes in transcription, translation or both in MIA males and females relative to sex-matched PBS controls (Fig. 4d–f). Both male and female MIA offspring showed reduced translation of *Eif4b*, which is an important regulator of cap-dependent translation[32] (Fig. 4d,e). Additionally, both male and female MIA offspring demonstrated reduced translation of the transcription initiation factor *Taf15*, thereby suggesting a negative effect on global transcription[33] (Fig. 4d,e). Conversely, MIA females showed significantly increased

translation of *Chd1*, which encodes a chromatin remodeler, whereas translation of *Chd1* was significantly decreased in MIA males (Fig. 4d,e). *Chd1* is necessary for nucleosomal dynamics during stress, and impairment in CHD1 function may contribute to neurodegeneration[34]. We also observed a number of sex-dependent translation events among ISR downstream target genes that might contribute to female resiliency to MIA. For example, female MIA offspring had significantly increased translation of *Eif4g2*, whereas there was no significant change in translation in male MIA offspring (Fig. 4f). *Eif4g2* encodes the protein DAP5 and is an alternative translation initiation factor that promotes cap-independent translation[35,36]. Both males and females demonstrated reduced translation of *Eif5b* with MIA, but this decrease was significantly greater in male MIA offspring (Fig. 4f). *Eif5b* is important for translation when eIF2α is phosphorylated in stress conditions[37].

In summary, MIA offspring—both male and female—exhibit profound changes in mRNA translation, but female offspring exhibit distinct translational differences that may promote adaptation and resiliency to intrauterine inflammation.

Blockade of ISR activation attenuates excessive neural activity in MIA offspring. We next sought to determine whether attenuation of ISR activation could rescue MIA-associated neurobehavioral phenotypes. To genetically dampen ISR activation, we utilized mice harboring a knock-in allele in which eIF2α serine 51 is replaced with an alanine (*eIF2α*^{S51A}), rendering it refractory to ISR-induced phosphorylation and thus blocking ISR pathway activation[38]. We crossed wild-type (WT) B6 females with heterozygous *eIF2α*$^{S51A/+}$ males, then injected poly(I:C) to induce MIA at E12.5. We first examined the resulting levels of phosphorylated eIF2α in E18.5 cortices of WT or *eIF2α*$^{S51A/+}$ littermate MIA offspring. *eIF2α*$^{S51A/+}$ male MIA offspring showed similar levels of eIF2α phosphorylation to the WT offspring of control PBS-treated dams, thereby confirming an attenuation of the ISR in these animals (Fig. 5a). As expected, levels of phospho-PERK remained elevated in MIA *eIF2α*$^{S51A/+}$ offspring (Fig. 5a), which confirms that PERK functions upstream of eIF2α. Accordingly, we also confirmed that decreased nascent protein synthesis in the WT MIA offspring was reversed in the cortex of *eIF2α*$^{S51A/+}$ littermate MIA offspring (Fig. 5b).

MIA offspring have previously been shown to display an abnormal increase in cortical neural activity, as measured by c-Fos, in the primary somatosensory cortex, including its dysgranular zone (S1DZ)[10]. Optogenetic modulation of neural activity in S1DZ regulates social preference in MIA offspring[10]. We tested whether ISR blockade also rescued the aberrant increase in cortical c-Fos. We confirmed that male MIA offspring demonstrated an increase in c-Fos expression in the cortex compared with male PBS offspring (Fig. 5c). By contrast, male *eIF2α*$^{S51A/+}$ MIA offspring exhibited a statistically significant reduction in cortical c-Fos expression compared with male WT offspring (Fig. 5c). MIA female offspring did not exhibit a significant change in c-Fos expression compared with PBS offspring (Extended Data Fig. 8a). This result supports a model in which the ISR is a central regulatory hub necessary for molecular phenotypes of MIA.

Blockade of ISR activation rescues the neurobehavioral phenotype in MIA offspring. We next examined the effects of ISR attenuation on MIA-induced behavioral abnormalities. Previous studies have demonstrated that MIA male offspring have reproducible deficits in sociability and repetitive behavior (marble burying)[9,10]. We performed behavioral assessment of *eIF2α*$^{S51A/+}$ and WT littermates from MIA and PBS control pregnancies. Consistent with prior results, WT MIA offspring demonstrated a loss of social preference compared with WT PBS offspring (Fig. 6a). *eIF2α*$^{S51A/+}$ MIA offspring showed normal social preference compared with littermate WT MIA offspring. Total distance moved, a measurement of activity or arousal during the sociability test, was indistinguishable between *eIF2α*$^{S51A/+}$ and WT littermates (Fig. 6b). In addition, WT MIA offspring exhibited increased marble-burying behavior, while *eIF2α*$^{S51A/+}$ MIA offspring exhibited similar marble-burying behavior to PBS offspring (Fig. 6c). MIA-driven behavioral abnormalities in the offspring were not present in the female offspring (Extended Data Fig. 8b,c).

To further corroborate the importance of the ISR to the behavioral phenotype in MIA male offspring, we treated pregnant dams with the ISR inhibitor ISRIB every other day after PBS or poly(I:C) injection. ISRIB rescues translation in the setting of eIF2α phosphorylation by promoting assembly of eIF2B[39–41]. The male MIA offspring from ISRIB-treated mothers exhibited normalization of social interaction and marble-burying behavior (Extended Data Fig. 9a,b). These data suggest that partial genetic and pharmacological blockade of the ISR are able to prevent MIA-associated behavioral abnormalities.

Discussion

In this study, we explored the mechanisms by which intrauterine inflammation shapes early neurodevelopment. We profiled the transcriptional and translational signatures of MIA and identified key pathways perturbed by intrauterine inflammation. Dysregulation of protein homeostasis (proteostasis) has previously been implicated in a wide variety of cognitive and neurodevelopmental disorders[42], and the coordination between protein synthesis and breakdown plays a critical role in the regulation of neural circuit development and synaptic plasticity[43,44]. Here, we showed that MIA exerts an intrauterine, sexually dimorphic effect on cell-type-specific transcription, with a disruption in genes associated with translation. These results have notable similarities to cell-type-specific transcriptional changes observed in the aging brain, including changes in ribosome-biogenesis-associated genes[45]. Our results also support the earlier findings of altered expression of translation initiation factors in the fetal brain in response to maternal lipopolysaccharide exposure[46]. Disruption of proteostasis may therefore be a common pathway in both neurodevelopmental and neurodegenerative disease.

In the present study, we identified activation of the ISR in male MIA offspring, and found that ISR activation is dependent on maternal IL-17a (and on gut bacteria promoting T_H17 cells), which sheds new mechanistic insight into the role of IL-17a in mediating MIA-associated neurodevelopmental disorders. We also demonstrated that activation of the ISR in MIA offspring is necessary for a core behavioral phenotype, as genetic attenuation of the ISR rescued social and repetitive behavioral dysfunction in MIA male offspring. We observed activation of PERK, an upstream eIF2α kinase, in male MIA offspring, which suggests that ER stress is a fundamental component of the early cellular response to MIA. This is in contrast to recent studies of a mouse model of Down syndrome, which identified PKR as the primary ISR-associated kinase[11]. Based on our results, we propose a model by which maternal-derived IL-17a triggers ER stress in the fetal cortex, thereby activating the ISR, arresting protein synthesis and promoting chronic, unresolved stress at this critical stage of neurodevelopment. Moreover, our data suggest that there is a sex-specific vulnerability to ISR activation in the fetal brain. While male offspring have a more prominent disruption of translation machinery than females, both male and female offspring exhibited transcriptional changes in response to MIA. Female offspring may possess resiliency factors that attenuate chronic stress, which warrants further study. The sexually dimorphic response to MIA has been previously described[16,17,47], and our results are consistent with prior reports suggesting sex-specific effects of intrauterine stress[48]. The present study adds molecular insight into this phenomena and expands our knowledge of sex-specific transcription in the developing brain at single-cell resolution. Additional studies are

necessary to elucidate the cellular mechanisms by which the male fetal brain is especially susceptible to IL-17a, including possible roles of intrauterine neuroendocrine signaling.

Online content

Any methods, additional references, Nature Research reporting summaries, source data, extended data, supplementary information, acknowledgements, peer review information; details of author contributions and competing interests; and statements of data and code availability are available at https://doi.org/10.1038/s41593-020-00762-9.

Received: 13 April 2020; Accepted: 18 November 2020;
Published online: 23 December 2020

References

1. Buffington, S. A. et al. Microbial reconstitution reverses maternal diet-induced social and synaptic deficits in offspring. *Cell* **165**, 1762–1775 (2016).
2. Hashimoto-Torii, K. et al. Roles of heat shock factor 1 in neuronal response to fetal environmental risks and its relevance to brain disorders. *Neuron* **82**, 560–572 (2014).
3. Gladwyn-Ng, I. et al. Stress-induced unfolded protein response contributes to Zika virus-associated microcephaly. *Nat. Neurosci.* **21**, 63–71 (2018).
4. Al-Haddad, B. J. S. et al. Long-term risk of neuropsychiatric disease after exposure to infection in utero. *JAMA Psychiatry* **76**, 594–602 (2019).
5. Atladóttir, H. O. et al. Maternal infection requiring hospitalization during pregnancy and autism spectrum disorders. *J. Autism Dev. Disord.* **40**, 1423–1430 (2010).
6. Patterson, P. H. Immune involvement in schizophrenia and autism: etiology, pathology and animal models. *Behav. Brain Res.* **204**, 313–321 (2009).
7. Lee, B. K. et al. Maternal hospitalization with infection during pregnancy and risk of autism spectrum disorders. *Brain. Behav. Immun.* **44**, 100–105 (2015).
8. Smith, S. E. P., Li, J., Garbett, K., Mirnics, K. & Patterson, P. H. Maternal immune activation alters fetal brain development through interleukin-6. *J. Neurosci.* **27**, 10695–10702 (2007).
9. Choi, G. B. et al. The maternal interleukin-17a pathway in mice promotes autism-like phenotypes in offspring. *Science* **351**, 933–939 (2016).
10. Shin Yim, Y. et al. Reversing behavioural abnormalities in mice exposed to maternal inflammation. *Nature* **549**, 482–487 (2017).
11. Zhu, P. J. et al. Activation of the ISR mediates the behavioral and neurophysiological abnormalities in Down syndrome. *Science* **366**, 843–849 (2019).
12. Larhammar, M. et al. Dual leucine zipper kinase-dependent PERK activation contributes to neuronal degeneration following insult. *eLife* **6**, e20725 (2017).
13. Green, K. M. et al. RAN translation at *C9orf72*-associated repeat expansions is selectively enhanced by the integrated stress response. *Nat. Commun.* **8**, 2005 (2017).
14. Cheng, W. et al. *C9ORF72* GGGGCC repeat-associated non-AUG translation is upregulated by stress through eIF2α phosphorylation. *Nat. Commun.* **9**, 51 (2018).
15. Loo, L. et al. Single-cell transcriptomic analysis of mouse neocortical development. *Nat. Commun.* **10**, 134 (2019).
16. Carlezon, W. A. et al. Maternal and early postnatal immune activation produce sex-specific effects on autism-like behaviors and neuroimmune function in mice. *Sci. Rep.* **9**, 16928 (2019).
17. Gogos, A., Sbisa, A., Witkamp, D. & van den Buuse, M. Sex differences in the effect of maternal immune activation on cognitive and psychosis-like behaviour in Long Evans rats. *Eur. J. Neurosci.* **52**, 2614–2626 (2020).
18. Rubio Gomez, M. A. & Ibba, M. Aminoacyl-tRNA synthetases. *RNA* **26**, 910–936 (2020).
19. Evers, R., Smid, A., Rudloff, U., Lottspeich, F. & Grummt, I. Different domains of the murine RNA polymerase I-specific termination factor mTTF-I serve distinct functions in transcription termination. *EMBO J.* **14**, 1248–1256 (1995).
20. Lessard, F., Stefanovsky, V., Tremblay, M. G. & Moss, T. The cellular abundance of the essential transcription termination factor TTF-I regulates ribosome biogenesis and is determined by MDM2 ubiquitinylation. *Nucleic Acids Res.* **40**, 5357–5367 (2012).
21. Pitale, P. M., Gorbatyuk, O. & Gorbatyuk, M. Neurodegeneration: keeping ATF4 on a tight leash. *Front. Cell. Neurosci.* **11**, 410 (2017).
22. Schmidt, E. K., Clavarino, G., Ceppi, M. & Pierre, P. SUnSET, a nonradioactive method to monitor protein synthesis. *Nat. Methods* **6**, 275–277 (2009).
23. Pakos-Zebrucka, K. et al. The integrated stress response. *EMBO Rep.* **17**, 1374–1395 (2016).
24. Ounallah-Saad, H., Sharma, V., Edry, E. & Rosenblum, K. Genetic or pharmacological reduction of PERK enhances cortical-dependent taste learning. *J. Neurosci.* **34**, 14624–14632 (2014).
25. Hetz, C. & Papa, F. R. The unfolded protein response and cell fate control. *Mol. Cell* **69**, 169–181 (2018).
26. Kim, S. et al. Maternal gut bacteria promote neurodevelopmental abnormalities in mouse offspring. *Nature* **549**, 528–532 (2017).
27. Lammert, C. R. et al. Cutting edge: critical roles for microbiota-mediated regulation of the immune system in a prenatal immune activation model of autism. *J. Immunol.* **201**, 845–850 (2018).
28. Ryoo, H. D. & Vasudevan, D. Two distinct nodes of translational inhibition in the integrated stress response. *BMB Rep.* **50**, 539–545 (2017).
29. Rojas, M., Vasconcelos, G. & Dever, T. E. An eIF2α-binding motif in protein phosphatase 1 subunit GADD34 and its viral orthologs is required to promote dephosphorylation of eIF2α. *Proc. Natl Acad. Sci. USA* **112**, E3466–E3475 (2015).
30. McGlincy, N. J. & Ingolia, N. T. Transcriptome-wide measurement of translation by ribosome profiling. *Methods* **126**, 112–129 (2017).
31. Calviello, L. et al. Detecting actively translated open reading frames in ribosome profiling data. *Nat. Methods* **13**, 165–170 (2016).
32. Merrick, W. C. Eukaryotic protein synthesis: an in vitro analysis. *Biochimie* **76**, 822–830 (1994).
33. Hoffmann, A. & Roeder, R. G. Cloning and characterization of human TAF20/15. Multiple interactions suggest a central role in TFIID complex formation. *J. Biol. Chem.* **271**, 18194–18202 (1996).
34. Berson, A. et al. TDP-43 promotes neurodegeneration by impairing chromatin remodeling. *Curr. Biol.* **27**, 3579–3590.e6 (2017).
35. Marash, L. et al. DAP5 promotes cap-independent translation of Bcl-2 and CDK1 to facilitate cell survival during mitosis. *Mol. Cell* **30**, 447–459 (2008).
36. Henis-Korenblit, S. et al. The caspase-cleaved DAP5 protein supports internal ribosome entry site-mediated translation of death proteins. *Proc. Natl Acad. Sci. USA* **99**, 5400–5405 (2002).
37. Terenin, I. M., Dmitriev, S. E., Andreev, D. E. & Shatsky, I. N. Eukaryotic translation initiation machinery can operate in a bacterial-like mode without eIF2. *Nat. Struct. Mol. Biol.* **15**, 836–841 (2008).
38. Scheuner, D. et al. Translational control is required for the unfolded protein response and in vivo glucose homeostasis. *Mol. Cell* **7**, 1165–1176 (2001).
39. Sidrauski, C. et al. Pharmacological brake-release of mRNA translation enhances cognitive memory. *eLife* **2**, e00498 (2013).
40. Sidrauski, C. et al. Pharmacological dimerization and activation of the exchange factor eIF2B antagonizes the integrated stress response. *eLife* **4**, e07314 (2015).
41. Sekine, Y. et al. Stress responses. Mutations in a translation initiation factor identify the target of a memory-enhancing compound. *Science* **348**, 1027–1030 (2015).
42. Chen, Y.-C., Chang, Y.-W. & Huang, Y.-S. Dysregulated translation in neurodevelopmental disorders: an overview of autism-risk genes involved in translation. *Dev. Neurobiol.* **79**, 60–74 (2019).
43. Alvarez-Castelao, B. & Schuman, E. M. The regulation of synaptic protein turnover. *J. Biol. Chem.* **290**, 28623–28630 (2015).
44. Costa-Mattioli, M., Sossin, W. S., Klann, E. & Sonenberg, N. Translational control of long-lasting synaptic plasticity and memory. *Neuron* **61**, 10–26 (2009).
45. Ximerakis, M. et al. Single-cell transcriptomic profiling of the aging mouse brain. *Nat. Neurosci.* **22**, 1696–1708 (2019).
46. Lombardo, M. V. et al. Maternal immune activation dysregulation of the fetal brain transcriptome and relevance to the pathophysiology of autism spectrum disorder. *Mol. Psychiatry* **23**, 1001–1013 (2018).
47. Braun, A. E. et al. "Females are not just 'protected' males': sex-specific vulnerabilities in placenta and brain after prenatal immune disruption. *eNeuro* https://doi.org/10.1523/ENEURO.0358-19.2019 (2019).
48. Sutherland, S. & Brunwasser, S. M. Sex differences in vulnerability to prenatal stress: a review of the recent literature. *Curr. Psychiatry Rep.* **20**, 102 (2018).
49. Guan, B.-J. et al. A unique ISR program determines cellular responses to chronic stress. *Mol. Cell* **68**, 885–900.e6 (2017).

Methods

Animals. All animals were housed in a specific pathogen-free facility with 20–22 °C, 40–55% humidity and 12-h light/12-h dark cycle. All experiments were conducted in accordance with procedures approved by the Institutional Animal Care and Use Committees of Harvard University. All WT C57BL/6 mice were obtained from Taconic Biosciences except for those used in experiments presented in Extended Data Fig. 7 (which were from The Jackson Laboratory). The generation and validation of *eIF2α*$^{S51A/+}$ mice has been previously described[38].

MIA. Mice were mated overnight with 8–12-week-old C57BL/6 females carrying a mouse commensal SFB[26,27]. For the experiments presented in Extended Data Fig. 7, both C57BL/6 males and females were directly purchased from The Jackson laboratory, mated overnight and maintained as SFB-free. To generate WT and *eIF2α*$^{S51A/+}$ littermates, we mated WT C57BL/6 Taconic females with SFB-positive *eIF2α*$^{S51A/+}$ males. On E12.5, pregnant mice were weighed and injected with a single dose (20 mg per kg, intraperitoneal injection) of poly(I:C) (P9582 or P1530, Sigma Aldrich) or PBS. Each dam was returned to its cage and left undisturbed until the birth of her litter. All pups remained with the mother until weaning on postnatal days 21–28, at which time mice were group-housed at a maximum of five per cage with same-sex littermates. For collecting embryonic tissues, pregnant dams were killed either on E14.5 or E18.5. Embryonic cortices were freshly dissected and processed. For the IL-17 cytokine blockade experiment, a monoclonal IL-17a-blocking antibody (clone 50104, R&D) or an isotype control antibody (IgG2a, clone 54447, R&D) was intraperitoneally injected (500 µg per animal) 5 h before MIA. For ISRIB treatment, pregnant mice were injected with 2.5 mg per kg ISRIB or vehicle followed by PBS or poly(I:C) injection every 2 days from E12.5 to E18.5 as previously described[11]. Sex of the embryos was determined by PCR of the *Sry* gene (forward: 5′- ACAAGTTGGCCCAGCAGAAT-3′, reverse: 5′-GGGATATCAACAGGCTGCCA-3′).

scRNA-seq. Samples were processed for scRNA-seq as previously described[50]. Embryonic cortices at E14.5 and E18.5 were transferred to dissociation medium, which contained the following: HBSS (Life Technologies), 10 mM HEPES buffer (Sigma), 172 mg per liter kynurenic acid (Sigma), 0.86 g per liter $MgCl_2{\cdot}6H_2O$ (Sigma), 6.3 g per liter D-glucose (Sigma), 1 µM tetrodotoxin, 100 µM AP-V (Thermo Fisher Scientific), 5 µg ml^{-1} actinomycin D (Sigma), 10 µM triptolide (Sigma) and 10 µg ml^{-1} anicomycin (Sigma). This solution was saturated with 95% O_2 and 5% CO_2 and was pH-adjusted to 7.35 before use. Papain (20 U per ml; Worthington), pronase from *Streptomyces griseus* (1 mg ml^{-1}; Sigma), proteinase XXIII from *Aspergillus melleus* (3 mg ml^{-1}; Sigma) and DNase (2 mg ml^{-1}; Worthington) were added to the dissociation medium. Dissociation was carried out at 37 °C for 1 h. The samples were then triturated, filtered and spun at 300 × *g* for 5 min. The pellet was resuspended in trypsin inhibitor solution (dissociation medium with 1% BSA and 1% ovomucoid). Following gradient centrifugation (70 × *g* for 10 min), the cells were washed in dissociation medium containing 0.04% BSA and resuspended in dissociation medium containing 0.04% BSA and 15% OptiPrep (Sigma). Individual cells were captured and barcoded using the inDrops platform as previously described[51]. Briefly, single-cell suspensions were fed into a microfluidic device that packaged the cells with barcoded hydrogel microspheres and reverse transcriptase/lysis reagents. After cell encapsulation, primers were photoreleased by exposure to ultraviolet light. Indexed libraries were pooled and sequenced on a NextSeq 500 (Illumina).

scRNA-seq data analysis. Sequencing data were aligned to the genome and processed according to a previously published pipeline (https://github.com/indrops/indrops). Briefly, this pipeline was used to build a custom transcriptome from Ensembl GRCm38 genome and GRCm38.84 annotation using Bowtie 1.1.1, after filtering the annotation gtf file (gencode.v17.annotation.gtf filtered for feature_type="gene", gene_type="protein_coding" and gene_status="KNOWN"). Unique molecular identifiers were used to link sequence reads back to individual captured molecules. All steps of the pipeline were run using default parameters unless explicitly stated.

All cells were combined into a single dataset. All mitochondrial genes were filtered from the dataset. Cells with fewer than 250 or more than 2,500 unique genes were excluded. Cells were then clustered using the Seurat R package. The data were log-normalized and scaled to 10,000 transcripts per cell. Variable genes were identified using the following parameters: x.low.cutoff = 0.0125, x.high.cutoff = 3, y.cutoff = 0.5. We limited the analysis to the top 30 principal components. Clustering resolution was set to 1. Clusters containing fewer than 100 cells were discarded, as were clusters for which one sample accounted for greater than 30% of the cells. Doublets were removed using Scrublet, and the remaining cells were re-clustered[52]. The expression of known marker genes was used to assign each cluster to one of the main cell types. Clusters from each cell type were combined, and the Seurat-based clustering was repeated to characterize subtype diversity. The Seurat FindMarkers function was used to identify genetic markers of cellular subtypes.

Identification of differentially expressed genes in the scRNA-seq data. To identify differentially expressed genes by cell type, we performed a DGE analysis using edgeR (3.28.1)[53,54]. The analysis was conducted on each cell type and on certain unions of cell types with common traits. To detect sex-dependent effects of MIA on gene expression, the difference between the change in gene expression due to MIA in males and the same change in females was used. Next, pairwise comparisons were performed to measure the effect of MIA on gene expression in each sex and on the baseline differences between sexes without treatment. The data were modeled and normalized using a negative binomial distribution, and count data were normalized for gene length and read depth. Genes with FDR < 5% were considered statistically significant. GO analysis was performed using the PANTHER classification system (FDR < 0.05 for significant GO terms)[55].

Three-chamber social-approach assay. Male or female mice (8–12 weeks old) were tested for social behavior using a three-chamber social-approach paradigm. A day before the test, experimental mice were introduced into a three-chamber arena (50 × 35 × 30 cm) with only empty-object containment cages (circular metallic cages, Stoelting Neuroscience) for a 10-min acclimation phase. The following day, the mice underwent a 5-min exploration period with empty-object containment cages. Immediately after, the mice were confined to the center chamber, while a social object (an unfamiliar C57BL/6 male mouse) in one chamber and an inanimate object (a rubber object of a similar size as the social object) in the other chamber were placed. Barriers to the adjacent chambers were removed, and the experimental mice were given 10 min to explore both chambers and measured for approach behavior as interaction time (that is, sniffing and approach) with targets in each chamber (within 2 cm). Sessions were video-recorded, and the object exploration time and the total distance traveled were analyzed using the Noldus tracking system. A social preference score was calculated as the percentage of time spent investigating the social target out of the total exploration time of both objects[56]. Arenas and contents were thoroughly cleaned between testing sessions. Multiple social targets from different home cages were used for testing to prevent potential odorant confounds from target home cages.

Marble-burying test. Male or female mice (8–12 weeks old) were placed in a testing arena (arena size: 40 × 20 cm^2; bedding depth: 3 cm) containing 20 glass marbles, which were laid out in five rows of four marbles equidistant from one another. At the end of a 15-min exploration period, mice were gently removed from the testing cages and the number of marbles buried was recorded. A marble-burying index was scored as 1 for marbles covered >50% by bedding, 0.5 for around 50% covered, or 0 for anything less. The percentage of buried marbles is plotted on the *y* axis.

Immunoblotting. For immunoblot analyses, embryonic cortices were lysed in lysis buffer consisting of 1% Triton X-100, 150 mM NaCl, 50 mM Tris-HCl (pH 7.4), 1 mM EDTA, 0.25% sodium deoxycholate, 0.1% SDS, phosphatase inhibitor cocktail (Thermo Fisher Scientific) and protease inhibitor cocktail (Roche). Protein concentrations were determined using the bicinchoninic acid assay (Thermo Fisher Scientific). Proteins were denatured by the addition of SDS containing Laemmli sample buffer (Boston Bioproduct) and boiled for 5 min at 95 °C. Antibodies against the following proteins were obtained from the indicated sources: phospho-S6K (9205), S6K (9202), phospho-eIF2α (9721), eIF2α (9722), phospho-PERK (3179), PERK (5683), GCN2 (3302), IRE1α (3294), β-actin (4970), horseradish peroxidase (HRP)-conjugated anti-rabbit secondary antibodies (7074) (Cell Signaling); phospho-GCN2 (ab75836), phospho-PKR (ab32036) (Abcam); pIRE1α (NB100-2323), ATF6 (NBP1-40256) (Novus Biologicals); and PKR (18244-1-AP; Proteintech). All primary antibodies were used at 1:1,000 dilution in 10% blocking buffer (Thermo Fisher Scientific) in TBS-T (Tris-buffered saline, 0.1% Tween-20). The HRP-conjugated secondary antibody was used at 1:2,000 dilution. The density of the resulting bands was quantified using ImageJ (v.2.0.0).

SUnSET and click conjugation with TAMRA azide. Protein synthesis was measured using a modified SUnSET method, a non-radioactive labeling method to monitor protein synthesis, as previously described[22]. Briefly, the fetal cortex was microdissected and incubated for 1 h at room temperature in oxygenated (95% O_2, 5% CO_2) artificial cerebrospinal fluid (ACSF) followed by incubation at 32 °C for 1 h in oxygenated (95% O_2, 5% CO_2) ACSF. OPP (25 µM) was bath-applied to the slices for 20 min followed by a wash with untreated oxygenated ACSF. The slices were then snap-frozen on dry ice and stored at −80 °C until use. Frozen slices were lysed in homogenization buffer (1% Triton X-100, 150 mM NaCl, 50 mM Tris-HCl (pH 7.4) and protease inhibitor cocktail). OPP incorporation was detected by click chemistry (Invitrogen, C10276) according to the manufacturer's recommendations. After click conjugation with TAMRA azide, 20 µg of protein sample was treated with 6× Laemmli sample buffer and resolved by SDS–PAGE gels. The gel was visualized using a Bio-Rad ChemiDoc imaging system at an excitation wavelength of 647 nm, then stained with Coomassie blue reagent. The density of the resulting bands was quantified using ImageJ (v.2.0.0).

Ribosome profiling and RNA-seq. We employed a modified version of the ribosome-profiling protocol described by McGlincy et al.[30]. Flash-frozen embryonic brain tissue was thawed in 400 µl lysis buffer (150 mM NaCl, 20 mM Tris (pH 7.4), 5 mM $MgCl_2$, 1 mM dithiothreitol, 100 µg ml^{-1} cycloheximide, 1%

v/v Triton X-100 and 25 U per ml Turbo DNase I (Thermo Fisher Scientific)). Tissue was pipetted ten times in lysis buffer and incubated for 10 min on ice. Tissue was then triturated ten times through a 26-gauge needle. Lysate was clarified by centrifugation for 10 min at 20,000×*g* at 4 °C and supernatant was recovered. The RNA concentration was quantified using a Qubit RNA assay (Thermo Fisher Scientific). A total of 5% input was reserved, and total RNA was purified using a Direct-zol RNA MiniPrep kit (Zymo) with DNaseI treatment. RNA-seq libraries were prepared from 10 ng total RNA using a SMARTer Stranded Total RNA-Seq kit v2 (Takara) and sequenced on a Next-seq 500 using paired-end 2×37 nt sequencing runs.

For ribosome profiling, 1.5 µl RNase I (10 U per µl; Thermo Fisher Scientific) was added to lysate containing 30 µg RNA and incubated for 45 min at room temperature with gentle agitation. A total of 10 µl SUPERaseIn RNase inhibitor (20 U per µl; Thermo Fisher Scientific) was added after 45 min, and samples were transferred onto ice to stop nuclease digestion. Lysate was transferred to a polycarbonate ultracentrifuge tube and underlaid with 0.9 ml sucrose cushion (1 M sucrose, 20 U per ml SUPERaseIn in Polysome buffer, 150 mM NaCl, 20 mM Tris (pH 7.4), 5 mM $MgCl_2$, 1 mM dithiothreitol, 100 µg ml^{-1} cycloheximide). Ribosome-protected RNAs were pelleted by centrifugation at 52,000 r.p.m. at 4 °C for 2 h. Supernatant was removed and the pellet resuspended in 300 µl TRIzol reagent. RNA fragments were purified using a Direct-zol RNA MiniPrep kit (Zymo Research) and eluted in 100 µl RNase-free water. RNA was precipitated with one volume of isopropanol, 30 µg GlycoBlue and 100 mM sodium acetate (pH 5.5) (300 µl total volume) and chilled at −20 °C for at least 2 h or overnight. RNA was pelleted by centrifugation for 30 min at 20,000×*g*, 4 °C, the supernatant was removed and pellet air-dried for 10 min. Purified RNA was resuspended in 5 µl 10 mM Tris (pH 8) and RNA of 17–34 nucleotides in length was size-selected using a 15% TBE–urea gel (Life Technologies). RNA was extracted from gel sections in 400 µl RNA extraction buffer (300 mM sodium acetate (pH 5.5), 1 mM EDTA, 0.25% v/v SDS), then precipitated with 30 µg GlycoBlue and one volume of isopropanol. Precipitations were left at −20 °C overnight. Size-selected RNA was resuspended in 4 µl 10 mM Tris (pH 8) and transferred to a clean non-stick RNase-free microfuge tube. Size-selected RNA was dephosphorylated with T4 PNK (NEB) at 37 °C for 1 h. The reaction was brought up to 50 µl with nuclease-free water and purified using 1.8 volumes of Agencourt RNAClean XP beads (Beckman Coulter) and 5.4 volumes of isopropanol. Beads were captured on a magnetic rack and washed twice with 85% ethanol. Beads were air-dried and resuspended in 7 µl nuclease-free water. Supernatant containing purified RNA was removed from beads and quantified using a Qubit RNA assay (Thermo Fisher Scientific). Sequencing libraries were prepared using a SMARTer smRNA-Seq Kit for Illumina (Takara). Libraries were sequenced on a Novaseq 6000 using single-end 1×50 nt sequencing runs.

RNA-seq and ribosome-profiling libraries were analyzed in parallel. Reads were aligned to the mm10 genome using STAR (v.2.5.4a)[57]. Data were then analyzed by RibORF (v.1.0), which confirmed the periodicity of the ribo-seq data[58]. The RibORF script was run using SAM files, read lengths of 22, 28, 29 and 30 nucleotides, and an offset value of 12 nucleotides. Htseq (v.0.9.1)[59] was used with default parameters to generate raw count files from bam files for both RNA-seq and ribo-seq data. Counts were filtered to remove mitochondrial and ribosomal RNAs, and DGE analysis was performed using edgeR with the same scheme as the single-cell analysis. For ribosome-profiling reads, ribosomal RNA was filtered using Bowtie2 (v2.3.4.3)[60] followed by alignment of the non-ribosomal reads to the mm10 genome using STAR (v.2.5.4a)[57].

Immunohistochemistry. Mice were transcardially perfused with ice-cold PBS first and then with paraformaldehyde (PFA) (4% in PBS). Brains were kept in PFA overnight at 4 °C and moved to PBS until sectioned. Brains were submerged in PBS with 3% agarose and then sliced on a vibratome (Leica VT1000S) into 50-µm coronal sections. Coronal sections were washed three times with PBS containing 0.3% Triton X-100 (PBST) and blocked for 1 h at room temperature with PBST containing 5% donkey serum. Sections were incubated overnight at 4 °C with rabbit anti-Fos antibody 1:2,000 (Cedarlane, 226003(SY)), washed again three times with PBST and incubated for 1 h at room temperature with 1:500 donkey anti-rabbit 647 secondary antibody (Life Technologies, A31573). After washing in PBST and PBS, samples were mounted onto SuperFrost Plus glass slides (VWR) using 4,6-diamidino-2-phenylindole (DAPI) Fluoromount-G.

Images of brain slices were taken using a ×10 magnification lens on an Olympus VS-120 Slide Scanner with a 50-ms exposure time for the DAPI signal and a 3-s exposure time for the CY5 signal corresponding to the Alexa 647 secondary antibody. Image analysis was performed by an investigator blinded to the experimental conditions. CY5 signal images were loaded into ImageJ and reduced to include only fluorescent puncta using the native "adjust threshold" function. Brains with technical/quality issues were excluded. One cortical region of interest (ROI) from each side of the brain slice was drawn using the freehand ROI maker tool in ImageJ. The area within each drawn ROI was measured and recorded. Fluorescent puncta were automatically counted using the "analyze particles" function in ImageJ with a 0.7-circularity threshold and a 3-μm^2 size threshold to exclusively count biologically relevant fluorescent puncta. Of note, the analysis of male brain tissue (Fig. 5c) was performed independently from the analysis of female brain tissue (Extended Data Fig. 8a). Therefore, these results cannot be directly compared.

Statistics and reproducibility. No statistical methods were used to predetermine sample sizes, but the sample sizes were determined based on similar, previously conducted studies[10,11]. The data distribution was assumed to be normal, but this was not formally tested. Animals were randomized into different groups with approximately comparable numbers of animals in each group whenever possible. The analysis of c-Fos immunohistochemistry was performed by a blinded investigator. For the behavioral assays, experiments were run in a semi-blinded way, which means mice were numbered earlier at the weaning stage and their genotype information was matched after completion of the behavioral experiment. In the case of all the other experiments, investigators were not blinded during group allocation and data analyses due to the nature of the experiments. The statistical analyses were performed using GraphPad Prism software (v.8) using two-way analysis of variance (ANOVA) or one-way ANOVA followed by least significance difference post-hoc tests, or using Student's *t*-test, both two-sided. Details of specific statistical comparisons are listed in the relevant figure legends.

Reporting Summary. Further information on research design is available in the Nature Research Reporting Summary linked to this article.

Data availability

All the sequencing data that support the findings of this study have been deposited in the Gene Expression Omnibus with the accession code GSE148237. Publicly available datasets from PANTHER (http://pantherdb.org/) were used for the GO analysis. Source data are provided with this paper.

Code availability

All the custom code are available at https://github.com/bkalishneuro/Maternal-Immune-Activation-Project/blob/main/README.md.

References

50. Hrvatin, S. et al. Single-cell analysis of experience-dependent transcriptomic states in the mouse visual cortex. *Nat. Neurosci.* **21**, 120–129 (2018).
51. Klein, A. M. et al. Droplet barcoding for single-cell transcriptomics applied to embryonic stem cells. *Cell* **161**, 1187–1201 (2015).
52. Wolock, S. L., Lopez, R. & Klein, A. M. Scrublet: computational identification of cell doublets in single-cell transcriptomic data. *Cell Syst.* **8**, 281–291.e9 (2019).
53. Robinson, M. D., McCarthy, D. J. & Smyth, G. K. edgeR: a Bioconductor package for differential expression analysis of digital gene expression data. *Bioinformatics* **26**, 139–140 (2010).
54. McCarthy, D. J., Chen, Y. & Smyth, G. K. Differential expression analysis of multifactor RNA-seq experiments with respect to biological variation. *Nucleic Acids Res.* **40**, 4288–4297 (2012).
55. Thomas, P. D. et al. PANTHER: a library of protein families and subfamilies indexed by function. *Genome Res.* **13**, 2129–2141 (2003).
56. Nygaard, K. R., Maloney, S. E. & Dougherty, J. D. Erroneous inference based on a lack of preference within one group: autism, mice, and the social approach task. *Autism Res.* **12**, 1171–1183 (2019).
57. Dobin, A. et al. STAR: ultrafast universal RNA-seq aligner. *Bioinformatics* **29**, 15–21 (2013).
58. Ji, Z. RibORF: identifying genome-wide translated open reading frames using ribosome profiling. *Curr. Protoc. Mol. Biol.* **124**, e67 (2018).
59. Anders, S., Pyl, P. T. & Huber, W. HTSeq—a Python framework to work with high-throughput sequencing data. *Bioinformatics* **31**, 166–169 (2015).
60. Langmead, B. & Salzberg, S. L. Fast gapped-read alignment with Bowtie 2. *Nat. Methods* **9**, 357–359 (2012).

Acknowledgements

B.T.K. was supported by the Pediatric Scientist Development Program and the March of Dimes. E.K. was supported by the Basic Science Research Program through the National Research Foundation of Korea (NRF) funded by the Ministry of Education (2018R1A6A3A03010693). M.E.G. and B.T.K. were supported by R01 NS115965 from the National Institute of Neurological Disorders and Stroke. R.J.K. was supported by NIH grants R01CA198103-04, R01DK113171-03 and R01AG062190-02. E.E.D. was supported by the Damon Runyon Foundation. G.B.C. and J.R.H. were supported by the Jeongho Kim Neurodevelopmental Research Fund, the Simons Foundation Autism Research Initiative and National Institute of Mental Health grants (R01MH115037 and R01MH119459, respectively). J.R.H. was also supported by the PEW Scholars Program, the N of One: Autism Research Foundation and the Burroughs Wellcome Fund. Figures 1a, 3b and 4a were created using BioRender (https://biorender.com).

Author contributions

B.T.K., G.B.C., M.E.G. and J.R.H. conceptualized the study. B.T.K. and E.K. designed and performed the single-cell sequencing experiments. B.T.K., B.F. and E.E.D. performed

and analyzed the next-generation sequencing data. E.K. performed the immunoblotting and behavioral analyses. E.K., H.K. and Y.S.Y. bred mice for the experiments. C.K.G., L.T. and B.F. prepared tissues for histology and performed immunohistochemistry and microscopy. B.T.K., E.K., E.C.G., J.R.H. and M.E.G. wrote the manuscript. G.B.C., E.C.G., J.R.H. and M.E.G. provided guidance on the design of experiments and interpretation of results. R.J.K. provided *eIF2α*^{S51A} mice.

Competing interests

The authors declare no competing interests.

Additional information

Extended data is available for this paper at https://doi.org/10.1038/s41593-020-00762-9.

Supplementary information is available for this paper at https://doi.org/10.1038/s41593-020-00762-9.

Correspondence and requests for materials should be addressed to B.T.K., M.E.G. or J.R.H.

Peer review information *Nature Neuroscience* thanks Mauro Costa-Mattioli, John Lukens, and the other, anonymous, reviewer(s) for their contribution to the peer review of this work.

Reprints and permissions information is available at www.nature.com/reprints.

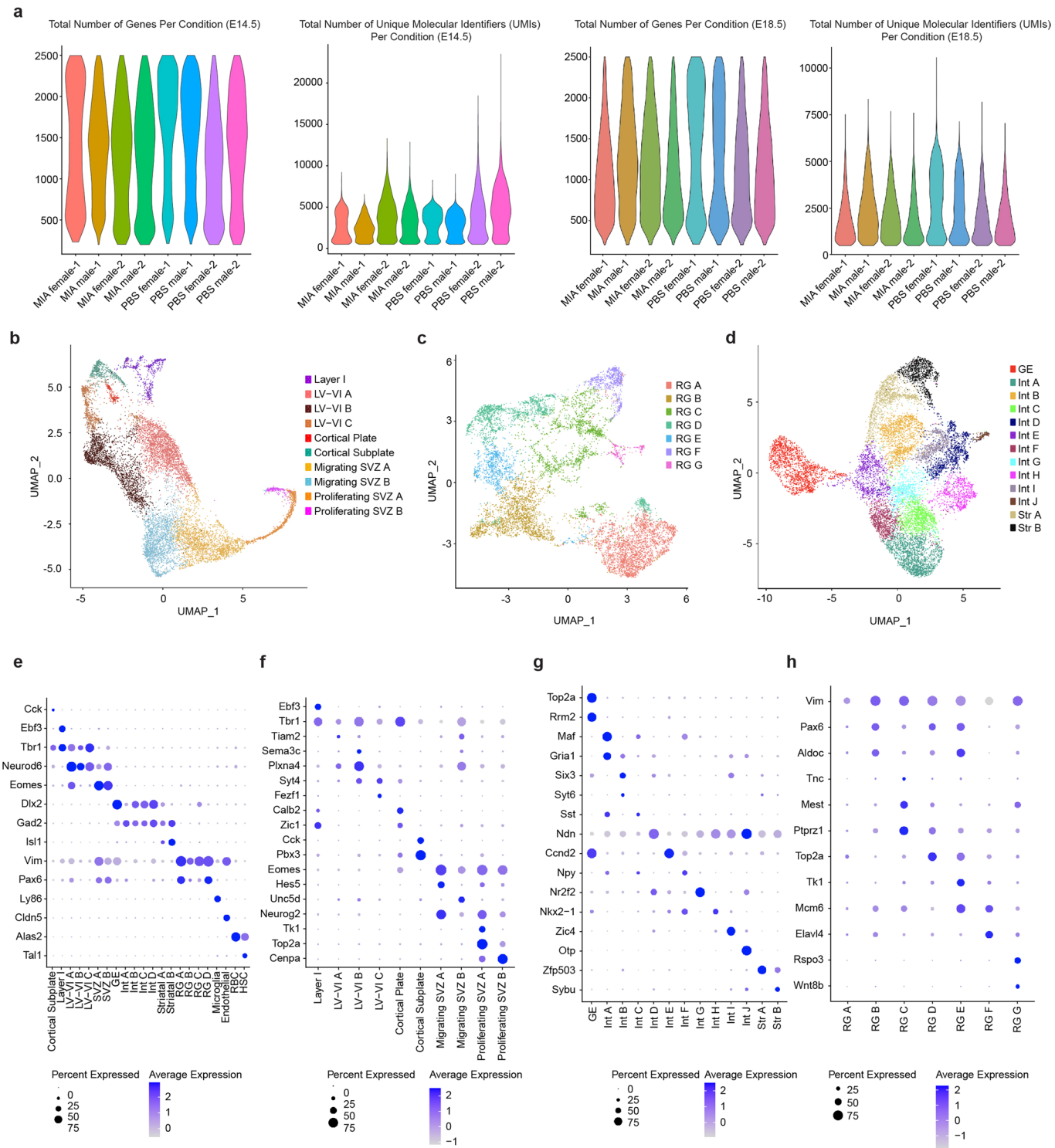

Extended Data Fig. 1 | Quality Control and E14.5 Sub-clustering. a, Total number of genes per condition and total number of unique molecular identifiers (UMIs) per condition in the final E14.5 and E18.5 single cell sequencing datasets. Data from $n = 2$ mice per group. **b**, UMAP of sub-clustering of mature and immature (SVZ, cortical plate, cortical subplate) neurons at E14.5. Data from $n = 2$ mice per group. **c**, UMAP of sub-clustering of radial glia (RG) at E14.5. Data from $n = 2$ mice per group. **d**, UMAP of sub-clustering of interneurons (Int), ganglionic eminence (GE), and striatal neurons at E14.5. Data from $n = 2$ mice per group. **e**, Dot plot of marker genes associated with all cells at E14.5. Data from $n = 2$ mice per group. **f**, Dot plot of marker genes associated with the cells in (b): mature and immature (SVZ, cortical plate, cortical subplate) neurons at E14.5. Data from $n = 2$ mice per group. **g**, Dot plot of marker genes associated with the cells in (d): interneurons (Int), ganglionic eminence (GE), and striatal neurons at E14.5. Data from $n = 2$ mice per group. **h**, Dot plot of marker genes associated with the cells in (c): radial glia (RG) at E14.5. Data from $n = 2$ mice per group.

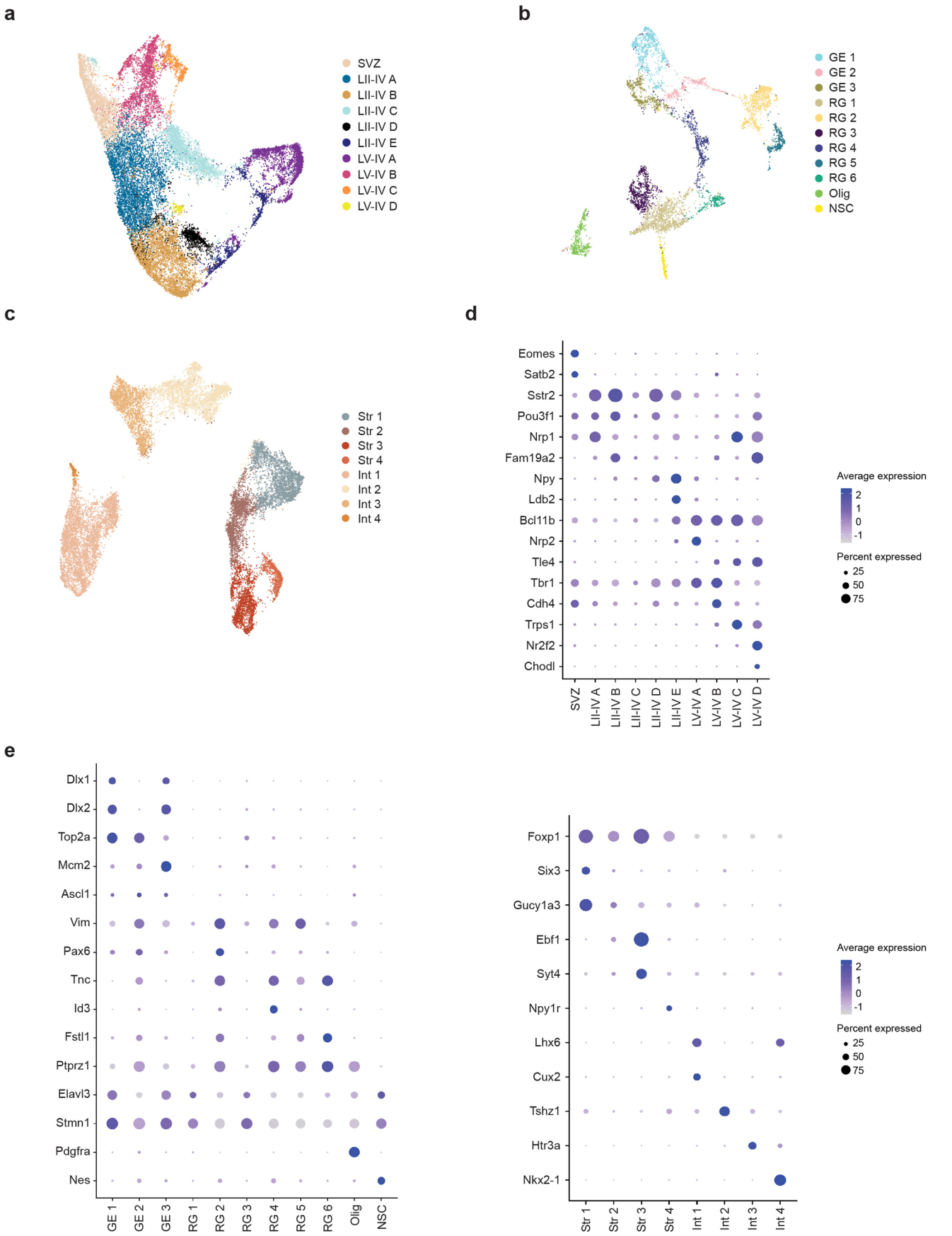

Extended Data Fig. 2 | See next page for caption.

Extended Data Fig. 2 | E18.5 sub-clustering. a, UMAP of sub-clustering of mature and immature (SVZ) neurons at E18.5. Data from $n = 2$ mice per group. **b**, UMAP of sub-clustering of radial glia (RG), ganglionic eminence (GE), oligodendrocytes (Olig), and neural stem cells (NSC) at E18.5. Data from $n = 2$ mice per group. **c**, UMAP of sub-clustering of striatal neurons (Str) and interneurons (Int) at E18.5. Data from $n = 2$ mice per group. **d**, Dot plot of marker genes associated with cells in (a): mature and immature (SVZ) neurons at E18.5. Data from $n = 2$ mice per group. **e, (left)** Dot plot of marker genes associated with cells in (b): radial glia (RG), ganglionic eminence (GE), oligodendrocytes (Olig), and neural stem cells (NSC) at E18.5; and **(right)** Dot plot of marker genes associated with cells in (c): striatal neurons (Str) and interneurons (Int) at E18.5. Data from $n = 2$ mice per group.

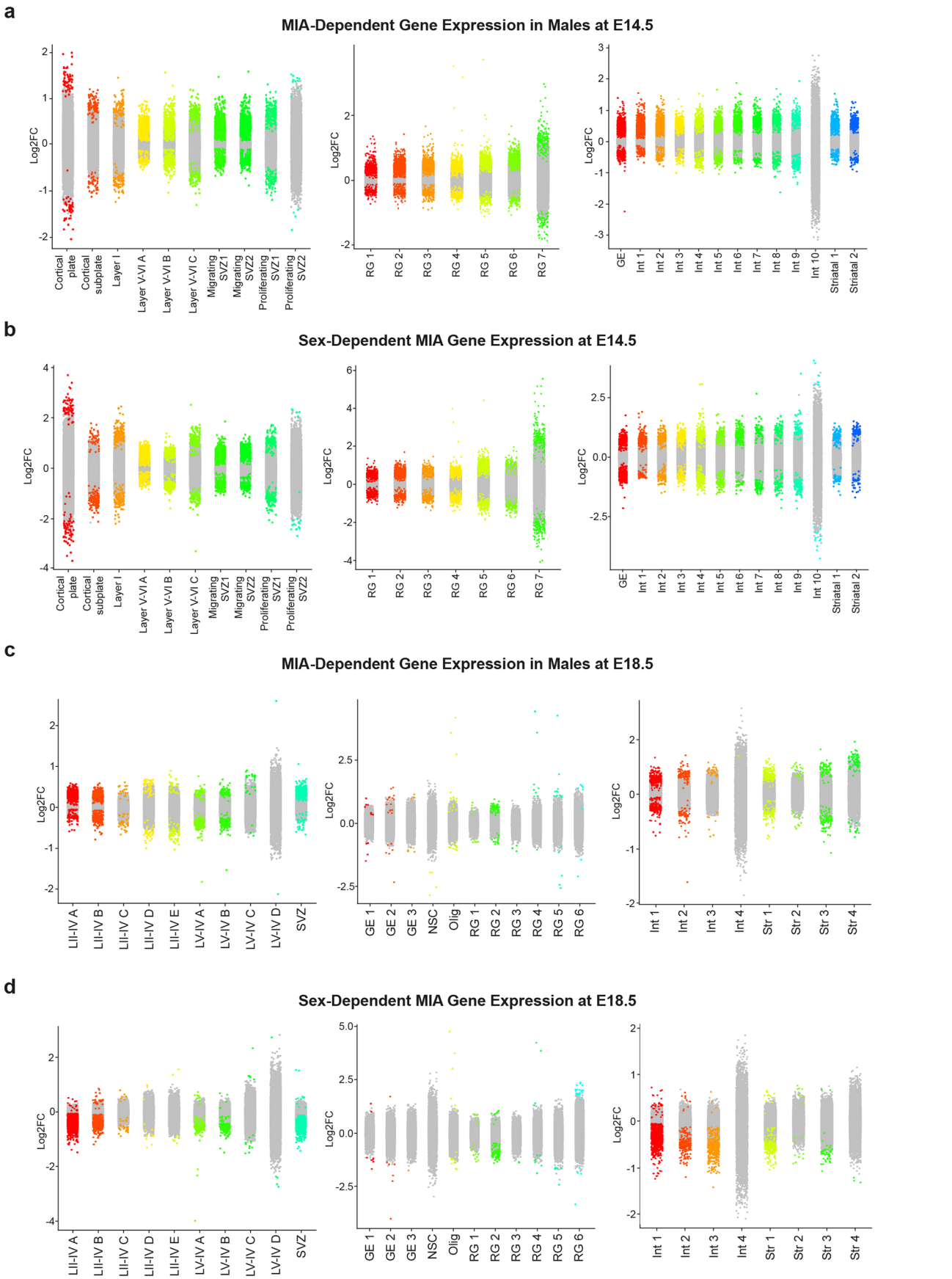

Extended Data Fig. 3 | See next page for caption.

Extended Data Fig. 3 | Differential gene expression strip plots. a, Strip plot displaying differential gene expression between MIA male offspring and PBS male offspring at E14.5. Colored dots represent significant genes (FDR < 0.05). The *x* axis displays select cortical cell types. Cell groups (left to right): (1) mature and immature (SVZ, cortical plate, cortical subplate) neurons, (2) radial glia (RG), and (3) interneurons (Int), ganglionic eminence (GE), and striatal neurons. Data from $n = 2$ mice per group. **b**, Strip plot displaying sex-dependent gene expression in MIA offspring at E14.5. Colored dots represent significant genes (FDR < 0.05). The *x* axis displays select cortical cell types. Cell groups (left to right): (1) mature and immature (SVZ, cortical plate, cortical subplate) neurons, (2) radial glia (RG), and (3) interneurons (Int), ganglionic eminence (GE), and striatal neurons. Data from $n = 2$ mice per group. **c**, Strip plot displaying differential gene expression between MIA male offspring and PBS male offspring at E18.5. Colored dots represent significant genes (FDR < 0.05). The *x* axis displays select cortical cell types. Cell groups (left to right): (1) mature and immature (SVZ) neurons, (2) radial glia (RG), ganglionic eminence (GE), oligodendrocytes (Olig), and neural stem cells (NSC), and (3) striatal neurons (Str) and interneurons (Int). Data from $n = 2$ mice per group. **d**, Strip plot displaying sex-dependent gene expression in MIA offspring at E18.5. Colored dots represent significant genes (FDR < 0.05). The *x* axis displays select cortical cell types. Cell groups (left to right): (1) mature and immature (SVZ) neurons, (2) radial glia (RG), ganglionic eminence (GE), oligodendrocytes (Olig), and neural stem cells (NSC), and (3) striatal neurons (Str) and interneurons (Int). Data from $n = 2$ mice per group.

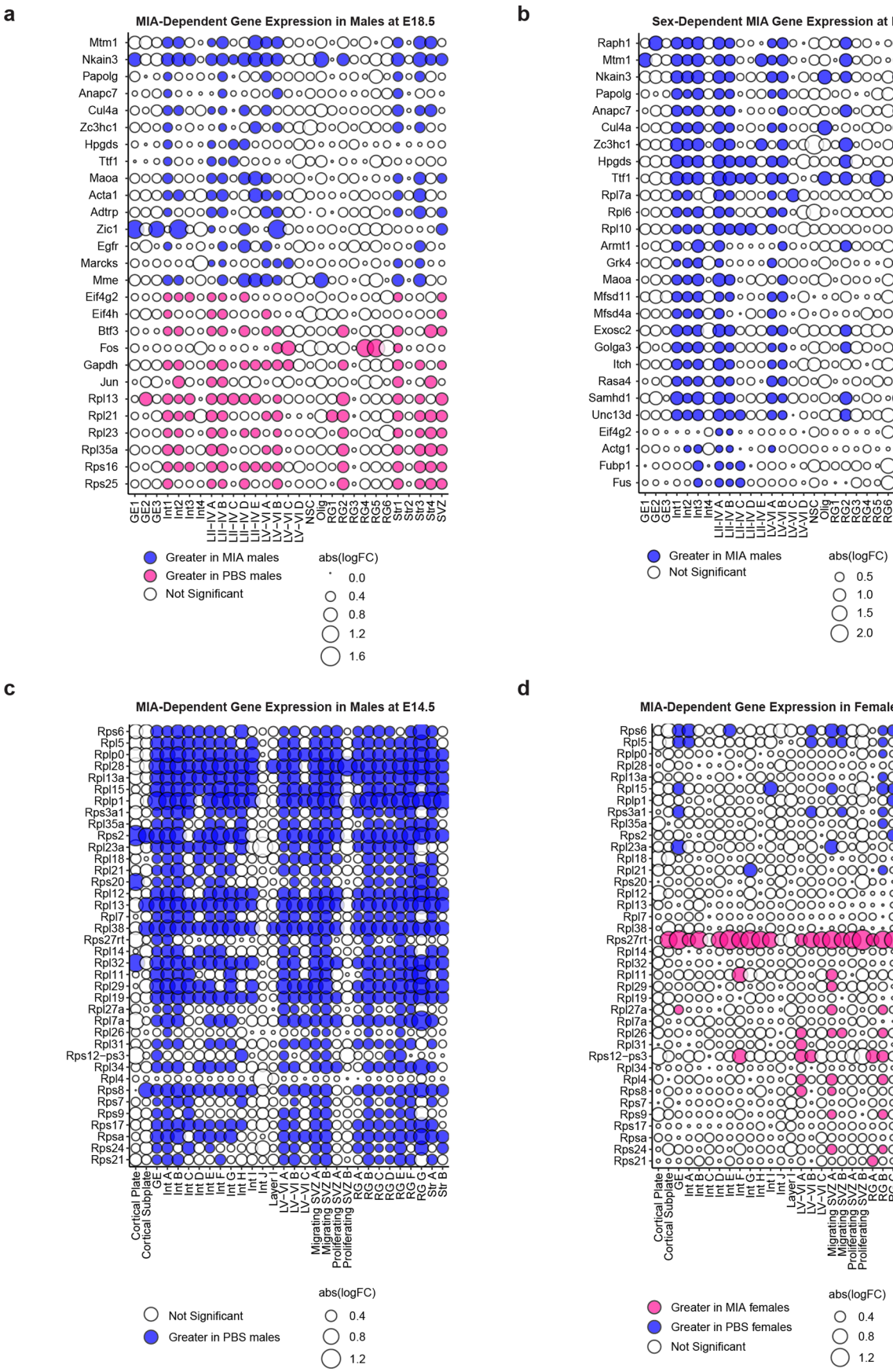

Extended Data Fig. 4 | See next page for caption.

Extended Data Fig. 4 | Single cell differential gene expression changes. a, Bubble plot of highly variable genes between MIA and PBS male offspring at E18.5. All significant genes FDR < 0.05. Blue indicates an increase in MIA males relative to PBS males. Data from $n = 2$ mice per group. **b**, Bubble plot of sex-dependent genes in MIA offspring at E18.5. All significant genes FDR < 0.05. Blue indicates an increase in Δ(MIA males – PBS males) relative to females. Data from $n = 2$ mice per group. **c**, Bubble plot of ribosome subunit genes between MIA male and PBS male offspring at E14.5, demonstrating a widespread decrease in expression of multiple ribosomal subunits in MIA male offspring. All significant genes FDR < 0.05. Blue indicates an increase in PBS males relative to MIA males. Data from $n = 2$ mice per group. **d**, Bubble plot of ribosome subunit genes between MIA female and PBS female offspring at E14.5, demonstrating an increase in expression of multiple ribosomal subunits in MIA female offspring. All significant genes FDR < 0.05. Blue indicates an increase in PBS females relative to MIA females. Data from $n = 2$ mice per group.

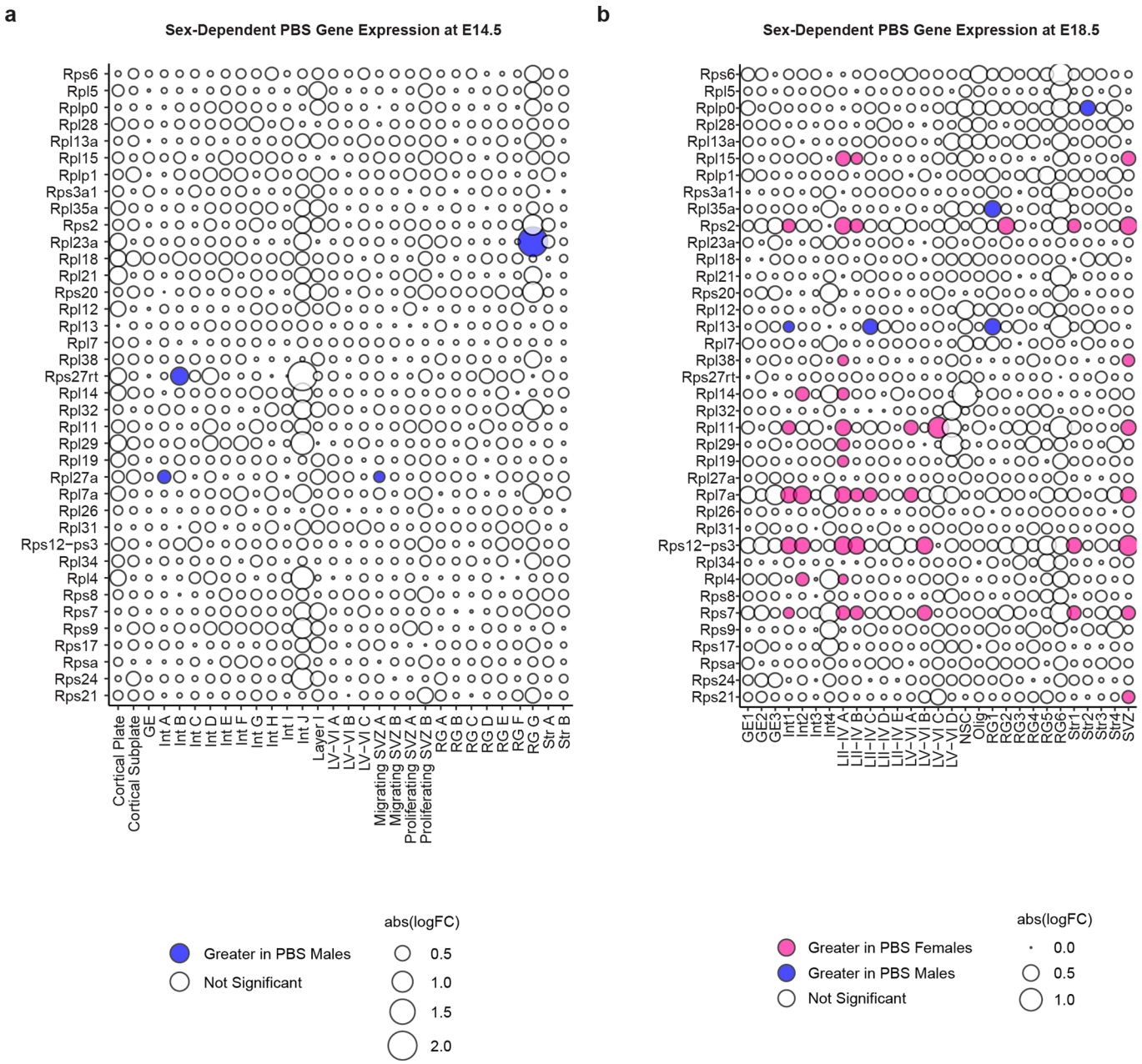

Extended Data Fig. 5 | Sex-specific comparisons in control (PBS) conditions. a, Bubble plot of ribosome subunit genes between PBS male and PBS female offspring at E14.5. All significant genes FDR < 0.05. Data from $n = 2$ mice per group. **b**, Bubble plot of ribosome subunit genes between PBS male and PBS female offspring at E18.5. All significant genes FDR < 0.05. Data from $n = 2$ mice per group.

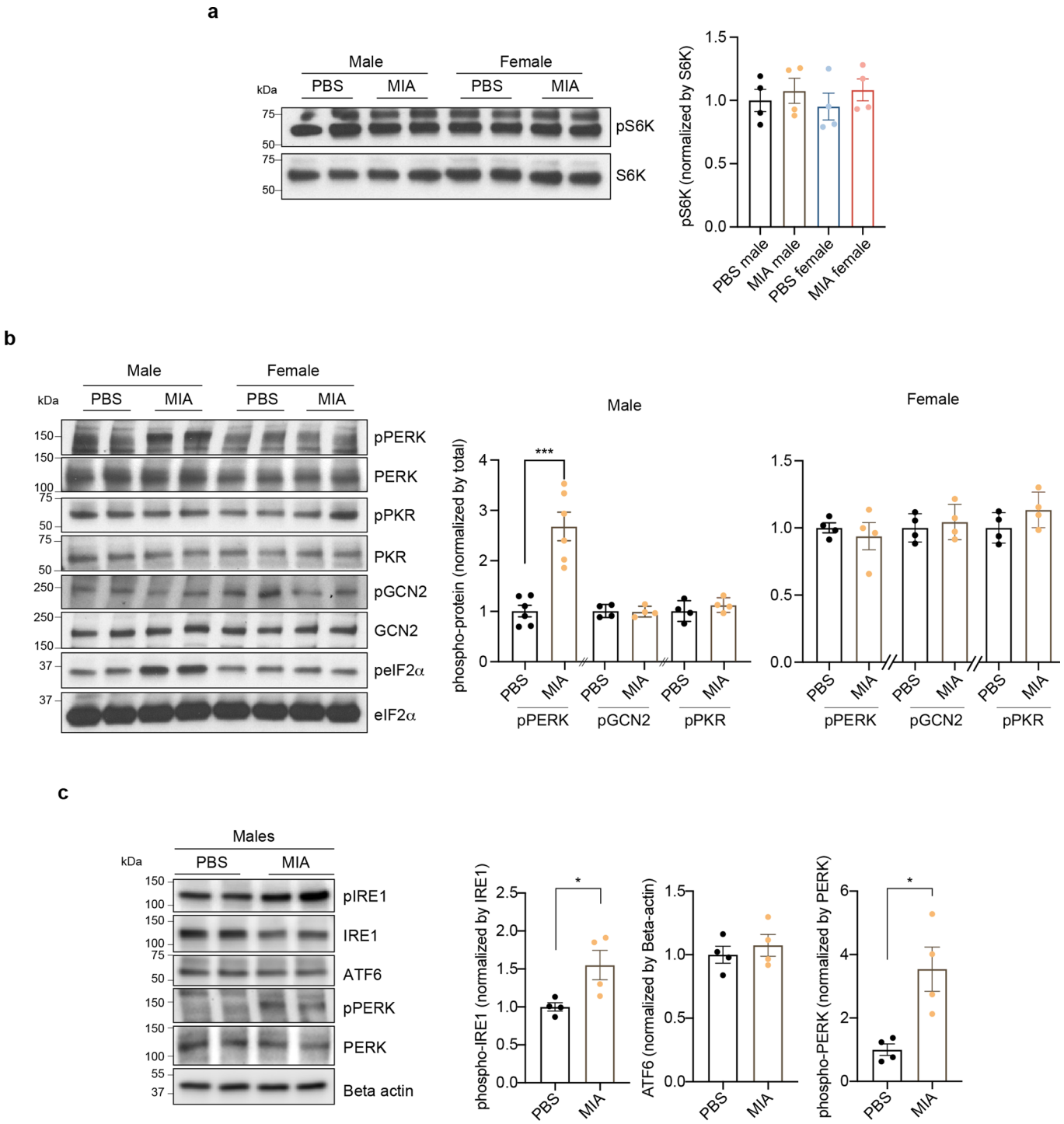

Extended Data Fig. 6 | Upstream regulators of phospho-eIF2α and UPR sensors in E18.5 PBS and MIA fetal cortices. a, Immunoblot analysis measuring phospho-S6K and quantification in E18 PBS and MIA fetal cortices. The *y* axis represents relative blot intensity to PBS male control (Two-way ANOVA sex (male or female) × stimulus (PBS or MIA) interaction $F_{1,12} = 0.08413$, $P = 0.7767$; effect of sex $F_{1,12} = 1.188$, $P = 0.2971$; effect of stimulus $F_{1,12} = 0.04729$, $P = 0.8315$ followed by Tukey multiple comparisons test; $n = 4$ pups from 2 litters). **b**, Immunoblot analysis measuring upstream regulators of phospho-eIF2α and quantification in E18.5 PBS and MIA fetal cortices. The *y* axis represents relative blot intensity to PBS control for each sex (Two-tailed unpaired *t*-test male: pPERK $t = 5.485$, $df = 10$, $^{***}P = 0.0003$, $n = 6$ from 3 litters; pGCN2 $t = 0.1503$, $df = 6$, $n = 4$ pups from 2 litters; pPKR $t = 0.9501$, $df = 6$, $n = 4$ pups from 2 litters; Two-tailed unpaired *t*-test female: pPERK $t = 0.5761$, $df = 6$; pGCN2 $t = 0.5204$, $df = 6$; pPKR $t = 1.545$, $df = 6$; $n = 4$ pups from 2 litters). **c**, Immunoblot analysis measuring UPR sensors (IRE1α, ATF6 and PERK) and quantification in E18.5 PBS and MIA male fetal cortices. The *y* axis represents relative blot intensity to PBS control (Two-tailed unpaired *t*-test: pIRE $t = 2.745$, $df = 6$, $^{*}P = 0.0335$; ATF6 $t = 0.6822$, $df = 6$; pPERK $t = 3.516$, $df = 6$, $^{*}P = 0.0126$; $n = 4$ pups from 2 litters). Data are mean ± s.e.m.; see Supplementary Table 20 for detailed statistics. Unprocessed blots are provided as a Source Data file.

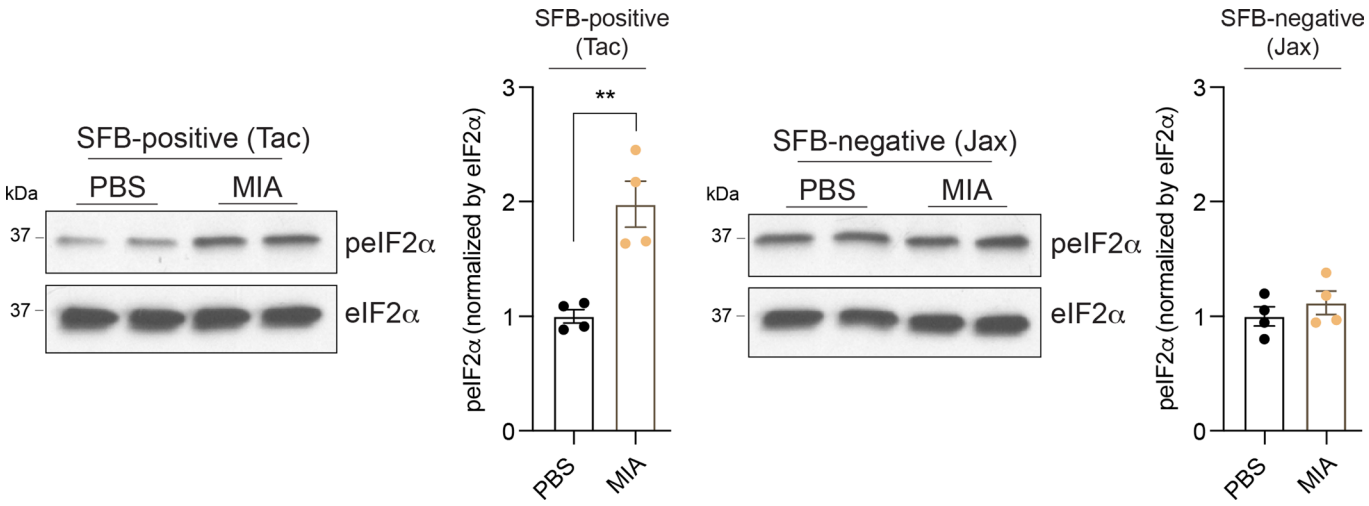

Extended Data Fig. 7 | ISR activation of E18.5 PBS and MIA male fetus in SFB-negative dams. Immunoblot analysis measuring phospho-eIF2α and quantification in E18.5 PBS and MIA male fetal cortices, either from SFB-positive or SFB-negative B6 dams. SFB-positive dams were obtained from Taconic Biosciences (Tac) whereas SFB-negative dams from Jackson laboratory (Jax) and maintained in SFB-positive and negative conditions, respectively. The *y* axis represents relative blot intensity to each PBS control (Two-tailed unpaired *t*-test: Tac $t = 4.659$, $df = 6$, $^{**}P = 0.0035$; Jax $t = 0.9013$, $df = 6$; $n = 4$ pups from 2 litters). Data are mean ± s.e.m.; see Supplementary Table 20 for detailed statistics. Unprocessed blots are provided as a Source Data file.

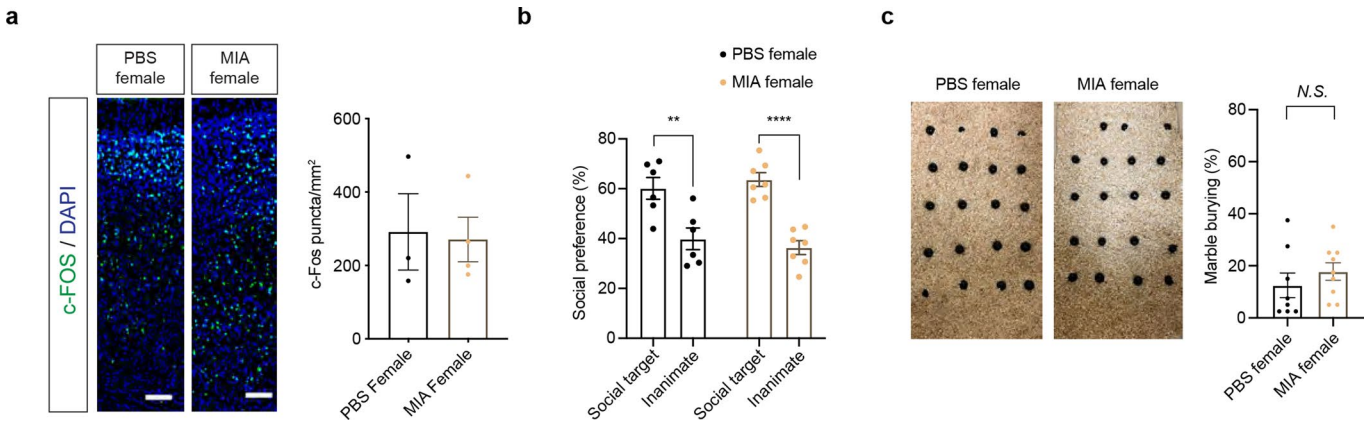

Extended Data Fig. 8 | Female MIA offspring neither show ISR activation nor neurodevelopmental abnormalities. a, Representative images of 8–10 weeks old MIA and PBS female offspring brain tissue immunostained for c-Fos. Scale bar 100 µm. Quantification indicates c-Fos puncta/mm^2 (Two-tailed unpaired *t*-test PBS female versus MIA female: $t = 0.1829$, $df = 5$, P = 0.8621; $n = 3$ for PBS female, $n = 4$ for MIA female mice). **b**, Percentage of interaction in the three-chamber sociability test of adult PBS and MIA female offspring littermates (Two-way ANOVA group (PBS female or MIA female) x preference to the target (social target or inanimate) interaction $F_{1,22} = 0.986$, $P = 0.3315$; effect of preference to the target $F_{1,22} = 45.24$, $P = 9.2454 \times 10^{-7}$ followed by Sidak multiple comparisons test-within group: PBS female ** $P = 0.0015$, MIA female **** $P = 2.06 \times 10^{-5}$; Two-tailed unpaired *t*-test social score between PBS female versus MIA female: $t = 0.7021$, $df = 11$, $P = 0.4972$; $n = 6$ for PBS female, $n = 7$ for MIA female mice; 2 independent experiments). **c**, Marble burying index of adult PBS and MIA female offspring littermates (Two-tailed unpaired *t*-test PBS female versus MIA female: $t = 0.9278$, $df = 15$, $P = 0.3682$; $n = 8$ for PBS female, $n = 9$ for MIA female mice; 2 independent experiments). Data are mean ± s.e.m.; see Supplementary Table 20 for detailed statistics.

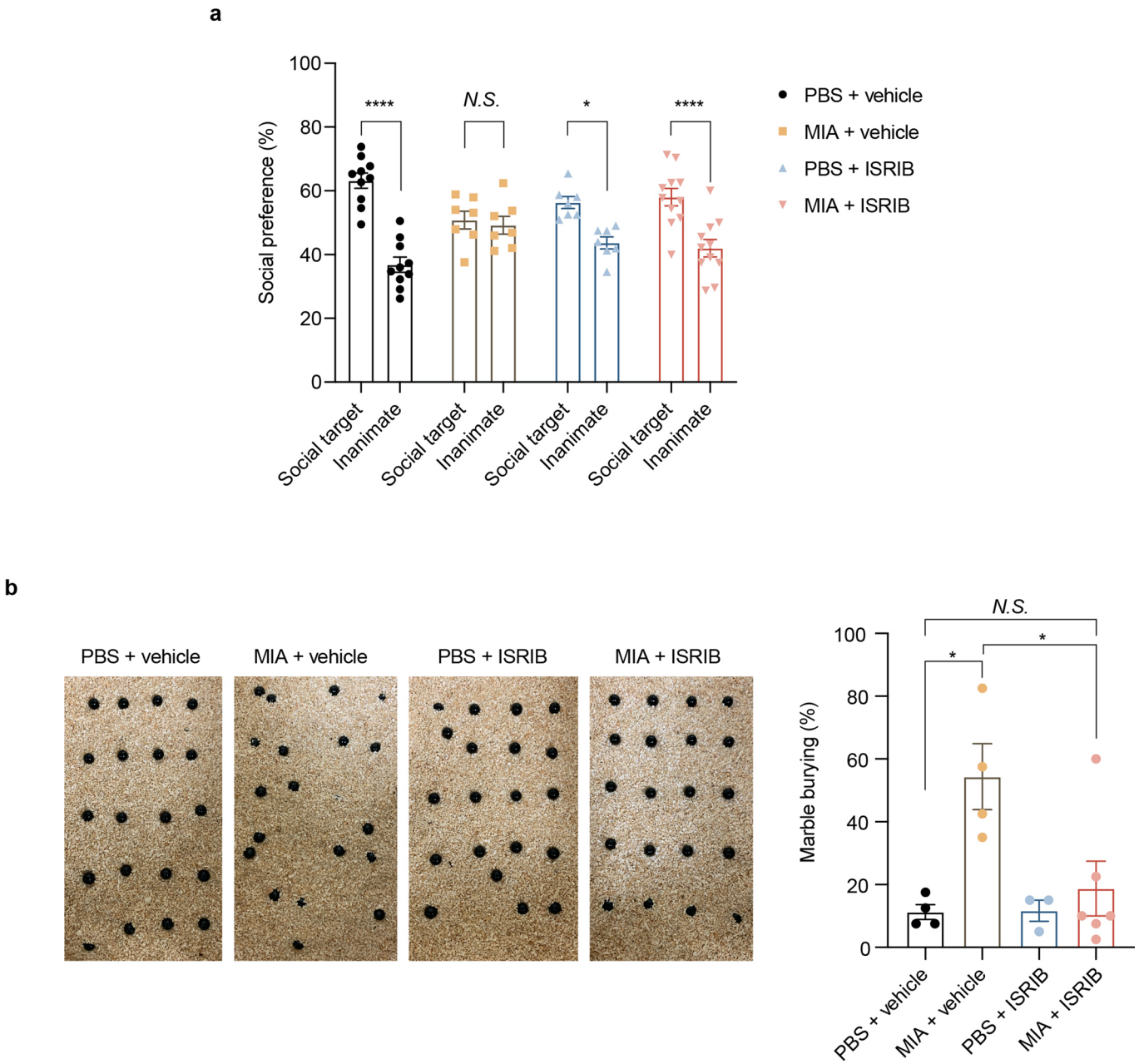

Extended Data Fig. 9 | Pharmacological inhibition of ISR protects MIA offspring from neurobehavioral abnormalities. a, Percentage of interaction in the three-chamber sociability test of vehicle and ISRIB-treated adult PBS and MIA offspring littermates (Two-way ANOVA group (PBS vehicle, MIA vehicle, PBS ISRIB or MIA ISRIB) x preference to the target (social target or inanimate) interaction $F_{3,62} = 7.401$, $P = 0.003$; effect of preference to the target $F_{1,62} = 57.62$, $P = 2\times10^{-10}$ followed by Bonferroni multiple comparisons test-within group: PBS vehicle **** $P = 4.9\times10^{-10}$, PBS ISRIB * $P = 0.0119$, MIA vehicle $P > 0.9999$, MIA ISRIB **** $P = 2.76\times10^{-5}$; two-way ANOVA stimulus (PBS or MIA) x treatment (vehicle or ISRIB) interaction $F_{1,31} = 7.111$, $P = 0.0121$; effect of stimulus $F_{1,31} = 4.109$, $P = 0.0513$; effect of treatment $F_{1,31} = 0.003618$, $P = 0.9524$ followed by Dunnett multiple comparisons test: PBS vehicle versus PBS ISRIB $P = 0.19$, MIA vehicle versus PBS vehicle **$P = 0.0071$, PBS vehicle versus MIA ISRIB $P = 0.3031$; $n = 10$ for PBS vehicle, $n = 7$ for MIA vehicle, $n = 7$ for PBS ISRIB, $n = 11$ for MIA ISRIB; 2 independent experiments). **b**, Marble burying index of vehicle and ISRIB-treated adult PBS and MIA offspring littermates (Two-way ANOVA stimulus (PBS or MIA) x treatment (vehicle or ISRIB) interaction $F_{1,13} = 4.549$, $P = 0.0526$; effect of stimulus $F_{1,13} = 8.829$, $P = 0.0108$; effect of treatment $F_{1,13} = 4.341$, $P = 0.0575$ followed by Tukey multiple comparisons test: PBS vehicle versus MIA vehicle *$P = 0.0147$, PBS ISRIB versus MIA vehicle *$P = 0.0255$, MIA vehicle vs. MIA ISRIB *$P = 0.0275$; $n = 4$ for PBS vehicle, $n = 4$ for MIA vehicle, $n = 3$ for PBS ISRIB, $n = 6$ for MIA ISRIB mice; 2 independent experiments). Data are mean ± s.e.m.; see Supplementary Table 20 for detailed statistics.

nature research

Corresponding author(s): Brian T. Kalish, Michael E. Greenberg, Jun R. Huh

Last updated by author(s): 11/10/2020

Reporting Summary

Nature Research wishes to improve the reproducibility of the work that we publish. This form provides structure for consistency and transparency in reporting. For further information on Nature Research policies, see Authors & Referees and the Editorial Policy Checklist.

Statistics

For all statistical analyses, confirm that the following items are present in the figure legend, table legend, main text, or Methods section.

n/a	Confirmed	
☐	☒	The exact sample size (*n*) for each experimental group/condition, given as a discrete number and unit of measurement
☐	☒	A statement on whether measurements were taken from distinct samples or whether the same sample was measured repeatedly
☐	☒	The statistical test(s) used AND whether they are one- or two-sided *Only common tests should be described solely by name; describe more complex techniques in the Methods section.*
☐	☒	A description of all covariates tested
☐	☒	A description of any assumptions or corrections, such as tests of normality and adjustment for multiple comparisons
☐	☒	A full description of the statistical parameters including central tendency (e.g. means) or other basic estimates (e.g. regression coefficient) AND variation (e.g. standard deviation) or associated estimates of uncertainty (e.g. confidence intervals)
☐	☒	For null hypothesis testing, the test statistic (e.g. *F*, *t*, *r*) with confidence intervals, effect sizes, degrees of freedom and *P* value noted *Give P values as exact values whenever suitable.*
☒	☐	For Bayesian analysis, information on the choice of priors and Markov chain Monte Carlo settings
☒	☐	For hierarchical and complex designs, identification of the appropriate level for tests and full reporting of outcomes
☒	☐	Estimates of effect sizes (e.g. Cohen's *d*, Pearson's *r*), indicating how they were calculated

Our web collection on statistics for biologists contains articles on many of the points above.

Software and code

Policy information about availability of computer code

Data collection	Noldus EthoVision XT (Noldus Information Technology)
Data analysis	Next-generation sequencing analysis code available at https://github.com/bkalishneuro/Maternal-Immune-Activation-Project/blob/main/README.md GraphPadPrism V8 (GraphPad Software) Noldus EthoVision XT ImageJ Software version 2.0.0 R Version 3.5.1 Seurat Version 3.0 Htseq Version 0.9.1 RibORF Version 1.0 Bowtie 1.1.1 EdgeR 3.28.1 STAR 2.5.4a

For manuscripts utilizing custom algorithms or software that are central to the research but not yet described in published literature, software must be made available to editors/reviewers. We strongly encourage code deposition in a community repository (e.g. GitHub). See the Nature Research guidelines for submitting code & software for further information.

Data

Policy information about availability of data

All manuscripts must include a data availability statement. This statement should provide the following information, where applicable:

- Accession codes, unique identifiers, or web links for publicly available datasets
- A list of figures that have associated raw data
- A description of any restrictions on data availability

Sequence data that support the findings of this study have been deposited in the Gene Expression Omnibus with the accession code GSE148237. Publicly available datasets from PANTHER (http://pantherdb.org/) were used for gene ontology analysis.

Field-specific reporting

Please select the one below that is the best fit for your research. If you are not sure, read the appropriate sections before making your selection.

☒ Life sciences ☐ Behavioural & social sciences ☐ Ecological, evolutionary & environmental sciences

For a reference copy of the document with all sections, see nature.com/documents/nr-reporting-summary-flat.pdf

Life sciences study design

All studies must disclose on these points even when the disclosure is negative.

Sample size	No statistical methods were used to predetermine sample size. Sample sizes were determined based on similar, previously conducted studies (main text ref. 10 and 11) and also magnitude and consistency of measurable differences. The precise number of animals used were indicated in the figure legends.
Data exclusions	For immunohistochemistry, images were excluded if immunostaining quality was poor or uneven. For ribosome profiling and RNA-sequencing, samples were selected based on quality metrics and sex-matching littermate controls. Data exclusion criteria were pre-established prior to complete data analysis.
Replication	All experiments were reproduced at least 2 times with independent batches of animals. Replication of studies statistically supported our conclusion in all experiments.
Randomization	Subject animals were randomly assigned to experimental groups.
Blinding	Analysis of c-Fos immunohistochemistry was performed by a blinded investigator. For the behavioral assays, experiments were run in a semi-blinded way, which means mice were numbered earlier at the weaning and their genotype information was matched after completion of the behavioral experiment. In the case of all other experiments, investigators were not blinded during group allocation and data analysis due to the nature of the experiments.

Reporting for specific materials, systems and methods

We require information from authors about some types of materials, experimental systems and methods used in many studies. Here, indicate whether each material, system or method listed is relevant to your study. If you are not sure if a list item applies to your research, read the appropriate section before selecting a response.

Materials & experimental systems

n/a	Involved in the study
☐	☒ Antibodies
☒	☐ Eukaryotic cell lines
☒	☐ Palaeontology
☐	☒ Animals and other organisms
☒	☐ Human research participants
☒	☐ Clinical data

Methods

n/a	Involved in the study
☒	☐ ChIP-seq
☒	☐ Flow cytometry
☒	☐ MRI-based neuroimaging

Antibodies

Antibodies used	Antibodies for Immunoblotting Polyclonal anti-phospho-S6K (Cell Signaling Technology, 9205, 1:1000) Polyclonal anti-S6K (Cell Signaling Technology, 9202, 1:1000) Polyclonal anti-phospho–eIF2α (Cell Signaling Technology, 9721, 1:1000) Polyclonal anti-eIF2α (Cell Signaling Technology, 9722, 1:1000)

Monoclonal (16F8) anti-phospho-PERK (Cell Signaling Technology, 3179, 1:1000)
Monoclonal (D11A8) anti-PERK (Cell Signaling Technology, 5683, 1:1000)
Polyclonal anti-GCN2 (Cell Signaling Technology, 3302, 1:1000)
Monoclonal (14C10) anti-IRE1α (Cell Signaling Technology, 3294, 1:1000)
Monoclonal (13E5) anti-Beta-Actin (Cell Signaling Technology, 4970, 1:1000)
Monoclonal (EPR2320Y) anti-phospho-GCN2 (Abcam, ab75836, 1:1000)
phospho-PKR (Abcam, ab32036, 1:1000)
PKR (Proteintech, 18244-1-AP, 1:1000)
pIRE1(Novus Biologicals, NB100-2323, 1:1000)
ATF6 (Novus Biologicals, NBP1-40256, 1:1000)
Horseradish peroxidase–conjugated anti-rabbit secondary antibodies (Cell Signaling Technology, 7074, 1:2000)

Antibodies for Immunohistochemistry
anti-Fos (Cedarlane, 226003(SY), 1:2000)
Donkey anti-rabbit 647 secondary antibody (Life Technologies, A31573, 1:500)

Antibodies for IL-17a neutralization
Monoclonal IL-17a blocking antibody (R&D systems, clone 50104, 500 µg/animal)
Isotype control antibody IgG2a (R&D systems, clone 54447, 500 µg/animal)

Validation

Antibodies for Immunoblotting
Polyclonal anti-phospho-S6K (Cell Signaling Technology, 9205, 1:1000): validated by the manufacturer for the application and species. See manufactures website for validation statement (www.cellsignal.com)
Polyclonal anti-S6K (Cell Signaling Technology, 9202, 1:1000): validated by the manufacturer for the application and species. See manufacturer's website for validation statement (www.cellsignal.com)
Polyclonal anti-phospho–eIF2α (Cell Signaling Technology, 9721, 1:1000): validated by the manufacturer for the application and species. See manufacturer's website for validation statement (www.cellsignal.com)
Polyclonal anti-eIF2α (Cell Signaling Technology, 9722, 1:1000): validated by the manufacturer for the application and species. See manufacturer's website for validation statement (www.cellsignal.com)
Monoclonal (16F8) anti-phospho-PERK (Cell Signaling Technology, 3179, 1:1000): application and species were validated in doi: 10.1016/j.neuron.2019.12.014
Monoclonal (D11A8) anti-PERK (Cell Signaling Technology, 5683, 1:1000): application and species were validated in doi: 10.1038/s41556-017-0006-y
Polyclonal anti-GCN2 (Cell Signaling Technology, 3302, 1:1000): validated by the manufacturer for the application and species. See manufacturer's website for validation statement (www.cellsignal.com)
Monoclonal (14C10) anti-IRE1α (Cell Signaling Technology, 3294, 1:1000): validated by the manufacturer for the application and species. See manufacturer's website for validation statement (www.cellsignal.com)
Monoclonal (13E5) anti-Beta-Actin (Cell Signaling Technology, 4970, 1:1000): validated by the manufacturer for the application and species. See manufacturer's website for validation statement (www.cellsignal.com)
Monoclonal (EPR2320Y) anti-phospho-GCN2 (Abcam, ab75836, 1:1000): application and species were validated in DOI: 10.1126/science.aaw5185
phospho-PKR (Abcam, ab32036, 1:1000): application and species were validated in DOI: 10.1126/science.aaw5185
PKR (Proteintech, 18244-1-AP, 1:1000): validated by the manufacturer for the application and species. See manufacturer's website for validation statement (www.ptglab.com)
pIRE1(Novus Biologicals, NB100-2323, 1:1000): validated by the manufacturer for the application and species. See manufacturer's website for validation statement (www.nbio.com)
ATF6 (Novus Biologicals, NBP1-40256, 1:1000): validated by the manufacturer for the application and species. See manufacturer's website for validation statement (www.nbio.com)
Horseradish peroxidase–conjugated anti-rabbit secondary antibodies (Cell Signaling Technology, 7074, 1:2000): validated by the manufacturer for the application and species. See manufacturer's website for validation statement (www.cellsignal.com)

Antibodies for Immunohistochemistry
anti-Fos (Cedarlane, 226003(SY), 1:2000): validated by the manufacturer for the application and species. See manufacturer's website for validation statement (https://sysy.com/product/226003)
Donkey anti-rabbit 647 secondary antibody (Life Technologies, A31573, 1:500): validated by the manufacturer for the application and species. See manufacturer's website for validation statement (https://www.thermofisher.com/antibody/product/Donkey-anti-Rabbit-IgG-H-L-Highly-Cross-Adsorbed-Secondary-Antibody-Polyclonal/A-31573)

Antibodies for IL-17a neutralization
Monoclonal IL-17a blocking antibody (R&D systems, clone 50104, 500 µg/animal): validated by the manufacture for the application and species. See manufactures website for validation statement (www.rndsystems.com)
Isotype control antibody IgG2a (R&D systems, clone 54447, 500 µg/animal): validated by the manufacture for the application and species. See manufactures website for validation statement (www.rndsystems.com)

Animals and other organisms

Policy information about studies involving animals; ARRIVE guidelines recommended for reporting animal research

Laboratory animals

All animals were housed in specific pathogen free (SPF) facility with 20-22?, 40-55% humidity and 12-hour light/12-hour dark cycle. C57BL/6 mice were purchased from Taconic Biosciences (B6-M and B6-F) or Jackson laboratory (000664) (USA). Eif2α S51A/+ mice were provided by Dr. Kaufman's lab at Sanford Burnham Prebys Medical Discovery Institute.
8 to 16-week-old male mice and 8 to 12-week-old female mice were used for timed mating. Their embryos were analyzed at E14.5 or E18.5. For behavioral experiments, 8 to 12-week-old male and female mice were tested.

Wild animals	This study did not involve the use of wild animals.
Field-collected samples	This study did not involve the use of the field-collected samples.
Ethics oversight	All mouse studies were performed in full compliance with IACUC approved protocol and guidelines of Harvard Medical School.

Note that full information on the approval of the study protocol must also be provided in the manuscript.